Light-Responsive, Steerable Hydrogel Micro-Crawlers.

Master Thesis - Charlie Maslen

Supervisors: Ivan Rehor & Willem Kegel

Van ’t Hoff Laboratory for Physical & Colloidal Chemistry,

Debye Institute for Nanomaterials Sciences, Utrecht University.

Contents

Abstract

Mimicking the crawling abilities of living organisms in robotics is a challenging feat, requiring complex feedback circuits to manage the many moving parts whilst retaining balance and precision. This is especially true on the microscale, where the downsizing of rigid parts and circuitry presents many new problems. In nature, it can be seen that many soft-bodied organisms have evolved strategies to spatiotemporally control friction between their bodies and environment in order to achieve locomotion. In this research, microscopic (100 μm) hydrogels are demonstrated to crawl by reciprocal actuation coupled to spatiotemporal modulation of friction between the gel and the surface. Thermo-responsive polyethylene glycol diacrylate (PEGDA) -crosslinked poly-n-isopropyl acrylamide (PNIPAm) gels are loaded with gold nanoparticles such that a localised shrinking response occurs when irradiated with laser light. Off-center modulation of the shrinking response, combined with a hysteresis in the friction of the gel between shrinking and expanding cycles, results in a crawling motion. Crawlers produced this way are demonstrated to be steerable and have the ability to push small cargo along a surface. The new principle of crawling enables designing soft micro-robots that can crawl by single degree of freedom actuation and have the potential to be further modified with sensors or other devices.

Keywords: **Microgel, Micro-crawler, Soft Robotics, Stop-flow Lithography, PNIPAm**

Light-Responsive, Steerable Hydrogel Micro-Crawlers

For millennia, humans have produced technologies which either automate the tasks we would do ourselves, or perform otherwise impossible tasks. The word to describe such technologies, robots, comes from the Czech word: *robota*, meaning slave labour. The word implies an abdication of work by humans which should be taken up by robotic technologies we develop. Simple technologies such as those found in a toolbox; screwdrivers, wrenches, nails etc. have long been replaced in industry with robots that are themselves the toolbox. Mass production of goods has been accelerated by the production of automated robots. Able to perform a multitude of tasks through design and programming, robots and their increasing efficiency will spread into all industries: healthcare, sustainable development, construction and many more. As they do so, some will be required to enable control on length-scales otherwise impossible for humans, sub-millimetre and lower in, for example, single cell analysis. Additionally, for many it will be a requirement that they do no damage to their environment and, as such, might be composed of soft materials. An example is given by the PneuNet soft gripper, that can lift up a chicken egg, not by incorporation of many feedback loops and circuitry, but by simply being softer than the egg[1]. A final point is that many robots would be greatly improved with an ability to locomote remotely. By introducing a robot in one location and navigating it to a more difficult or impossible to reach location, the difficulty of deployment in such a final location is avoided.

As technology develops at an accelerating pace, it does so on all length scales. Nanomaterials research has provided a bedrock of knowledge which should soon bring about technological developments that impact on the scales we interact with, namely the centimetre-metre range[2]. As nanomaterial research and the demand for macroscopically useful technologies

co-develop, they will converge and meetings will occur at the micro-scale[3]. Materials that are designed on the micro-scale may provide the step from which the properties of nanomaterials (often fascinatingly different to their macroscopic counterparts) can be propelled into 'real-life' applications. For example, optically active nanomaterials such as plasmonic particles can be ordered into microstructures. The properties of the resulting material then arise from the both the microscopic arrangement and the nanoscopic properties of the particles and can be tuned on both levels[4]. By tuning the microstructure, the optical properties of the nanoparticles may be enhanced collectively for use in light energy harvesting on macroscopic and potentially industrial scales.

Additionally, advancements in the modelling of active matter systems are not yet matched by experimental realisations on the micro-scale. Here 'active' refers to a self-driving property of the individual building blocks that make up the system. Most experimental realisations of active matter rely on Brownian motion or a large diffusive coefficient for active particles to swim, achievable only with sub-micron particles[5,6]. A physical technological toolkit must still be developed before the potential of such systems can be realised on larger scales. Large quantities of simple micro-robots that drive themselves by crawling may be excellent "autonomous agents in healthcare, sustainable construction and security"[6]. The collective activity of such a group of micro-crawlers would have properties far more complex than a singular micro-crawler, or a larger robot, which may have far-reaching technological applications[7].

The aim of this research is to utilise a microfabrication technique, stop-flow lithography, which can produce light-responsive hydrogel actuators composed of poly-N-isopropyl acrylamide (PNIPAm) embedded with gold nanoparticles, to develop soft, crawling microgels. The microgels produced can actuate through shrinking-expanding cycles when irradiated by modulated laser light – via photothermal heating of the gold nanoparticles. How this actuation can be converted into

directional motion will be the principle investigation. Additionally, upon the development of crawlers, their ability to perform tasks such as being steered, micro-manipulation and uphill climbing shall be investigated.

1 Soft, Responsive Materials for Robotics

1.1 Soft Robotics

Flexible and adaptive materials have been the subject of significant research for bio-mimetic robotics as well as mechanical actuators, microfluidics, artificial muscles and smart lenses[8]. The ability of a soft material to undergo shape changes in a response to external stimuli may bypass many of the problems associated with electronic, 'rigid' robots. For example, to maximise precision, many degrees of freedom are sacrificed in conventional robotics which leaves them very specialized to one function[9]. In contrast, biological organisms have one body and display incredible multifunctionality; octopi can open tightly shut clams, squeeze through tiny openings and locomote in both water and on land[10,11]. Octopi are an extreme example of soft animals, but the term also expands across many examples in nature: mice which are able to squeeze through tiny openings; worms which navigate through dense mud; and the human hand which can easily grip and hold small and delicate objects. All of these rely on the compliance of their bodies[9]. Mimicking these capabilities by the use of soft, compliant materials may provide an abundance of technological developments in various fields. In this research, attempts will be made to produce microscopic crawling robots using a soft, responsive material. The material is photothermally responsive PNIPAm hydrogel which actuates by shrinking and expanding in response to irradiation with green laser light.

1.1.1 Mimicking Nature.

In order to produce a crawler from a responsive microgel, it is first wise to examine the limitations of the material, find similarities in nature and then mimic the ways that nature exploits and thrives under such conditions.

With the responsive PNIPAm used in this research, come two major limitations. Firstly, there is only one degree of freedom in the actuation of the gel - it can only shrink and then expand along the same volumetric path. Secondly, the actuation of the gel is limited (by our method) in that it is localised around the centre of the irradiation, i.e. it is not possible to actuate the gel in more than one place at the same time. Additionally, in trying to produce any locomotors on the microscale, the hydrodynamics at such scales must be taken into account. In the so called low Reynold's regime, viscous forces dominate the system and place further limitations on the modes of locomotion (see section 1.1.3).

For organisms to locomote, the repeated shape changes (strokes) their body makes must result in a net non-zero force being exerted on the body. In the case of crawlers, the forces exerted are frictional[12,13]. In order to produce an imbalance, or directionality, in these forces, organisms have adopted two key strategies. The first is to employ non-reciprocal shape changes. Non-reciprocal meaning that the strokes are not symmetrical in time. For example, leeches and worms utilise a propagating wave of contraction along their body which modulates the friction between themselves and a surface – peristaltic motion. The direction of the propagating wave determines the direction of travel. Visualising the process in reverse, the wave direction is changed and the process is thus non-reciprocal.

Secondly, many organisms employ reciprocal shape changes which are coupled to spatiotemporal control of their points of adhesion. Inchworms use reciprocal shape changes of their body as they bend and stretch. Visualised in reverse, the actuation is identical. They couple this to alternating which side of their body is anchored to the surface by their legs, spatiotemporally controlling their points of adhesion[14].

It is possible to induce a wave of contraction by scanning the PNIPAm gel with the laser irradiation and so this shall be investigated. However, reciprocal shape changes will be much easier to demonstrate with PNIPAm gel as the shrinking-expanding cycle can be localised and the irradiation need not be dynamic.

1.1.2 Soft Crawlers.

Crawling has thus far been demonstrated in robotics on a range of length scales, from large scale load carrying robots to millimetre scale biomimetic worms[15,16]. The vast majority of such robots are constructed, at least partially, with rigid materials. For the purposes of this research, a distinction between said robots and 'pure' soft robots - containing no rigid parts - should be made. Examples of pure soft crawlers are much fewer in research though this is more likely due to the lowering costs of microelectronics and their commercial abundance than to the difficulty in producing soft materials. Some examples of the smallest pure, soft crawling robots will now be discussed.

The earliest found example of a truly soft crawler is a 2 cm long polymer strip, made to bend reversibly by the association and dissociation of charged surfactants under an external electric field[17]. The gel then moves by a combination of hooks on either end of the strip, attaching to or sliding over a ratcheted surface. A 1 cm long soft crawler has been developed by the joining of two electro-responsive hydrogel legs[18]. The crawler moves by alternating actuations of the legs, stimulated by external electric fields and could achieve a maximum velocity of ~2.5 mm/min. Another crawler, composed of a chemically responsive hydrogel that bends and straightens as a chemical wave propagates along its length[19]. The bending and straightening is similar to the gait of an inchworm but in this case the motion is achieved by actuation on a ratcheted surface. A similarly designed crawler has also been shown to carry cargo 125 times the crawler's dry weight

at velocities of 5 mm/min[20]. A common limitation for these crawlers is that they can only locomote in one direction and have no routes to steerability. This research will aim to utilise the freedom of design given by stop-flow lithography (section 1.3.1) to produce steerable crawlers in order to overcome this robotic limitation.

More examples of purely soft crawlers were not found which illustrates the gap in current research dedicated to the topic. Whilst combining soft materials with hard materials would surely yield a much broader range of robotic capabilities, that it could be possible to create a crawler from a single piece of soft material negates the need to incorporate extra components for locomotion. As such, there would be more freedom in the design to include components for other functions such as sensors.

1.1.3 Micro-Robotics.

Microrobots are characteristically less than 1 mm in at least one dimension, though the definition is never strictly followed[21]. Their dimensions make them ideal candidates for minimally invasive surgeries and targeted drug delivery and the ability of micromachines to navigate, untethered, to a target within a body is a minimum requirement for such applications[22,23]. Large numbers of microrobots may also be used in tissue engineering where the construction of micro-structured scaffolding is limited by the number of bio-materials available for lithographic techniques[24]. Programmable micro-robots that may deposit or degrade materials may be used as 'construction workers' or as building blocks themselves as they assemble micro-structures[25,26].

Locomoting by any means at the micro-scale and in aqueous environments comes with a limitation related to the scale. The 'Reynold's number' (*Re*) describes the ratio of the inertial forces to the viscous forces that act on a body in a given liquid environment. Described as follows:

$$Re = \frac{av\rho}{\eta} = \frac{av}{V^2}$$

Where a and v are the dimensions and velocity of the body respectively, and ρ and η are the density and viscosity of the liquid respectively. This can then be written in terms of V – the kinematic viscosity (10^{-2} cm^2s^{-1} for water). If Re is small (<1), then the viscous forces dominate the system and inertial forces are neglected[27]. That is to say; removal of the driving force acting on a body brings the body to an almost instantaneous halt. In the case of a generalised (large and fast) micro robot with dimensions $a \approx 0.01$ cm and travelling with velocity $v = 0.01$ cms^{-1}, then $Re = 10^{-2}$ which falls well into the low Reynold's regime. A particular effect of this regime is that reciprocal actuation cannot drive a swimming motion[28]. This limitation was the motivation for this research to investigate micro-*crawlers*, where the additional friction forces with a substrate can be utilised to drive motion.

1.2 PNIPAm as a Soft Material for Robotics

Poly-N-isopropyl Acrylamide (PNIPAm) is a thermo-responsive polymer. It is inversely soluble in that, above a critical solution temperature (CST) (32°C), it goes from hydrophilic and water-soluble to hydrophobic and water-insoluble[I,II]. Gels formed by crosslinking PNIPAm exhibit swelling and de-swelling behaviour as their temperature changes and water is absorbed or expelled in the hydrophilic and hydrophobic states respectively. A more detailed description of this phase transition can be found in section 1.2.1. The responsive properties of PNIPAm gels can be altered via different synthetic routes and these will be discussed in section 1.2.2. The swelling property

---

[I] PNIPAm in fact has a lower and upper critical solution temperature separated by a two-phase region. This is addressed in 1.2.1

[II] PNIPAm is never truly hydrophobic[29], though for the purposes of this research and want of a better term, 'hydrophobic' gives an adequate description of the behaviour.

can have many uses in actuation and drug-release and such applications will be explored in section 1.2.3.

1.2.1 Chemistry of PNIPAm and Formation of Hydrogels.

The phase transition of PNIPAm arises out of competition between the enthalpic and entropic terms in the Gibbs free energy[30]. At low temperatures, the negative enthalpy associated with the hydrogen bonding between water molecules and the polar amide group overcomes the decreased entropy associated with the hydration of the non-polar isopropyl and backbone regions[31]. As temperature increases, the entropic term of the Gibbs energy increases and at 32°C the increase in entropy by dissociation of water dominates the Gibbs free energy. The CST is in fact split into lower and upper critical solution temperatures (LCST and UCST respectively) with an intermediate two phase region[30]. Below the LCST the polymers exist in a flexible and expanded coil conformation and above the UCST they transition to a tightly packed globular state[32].

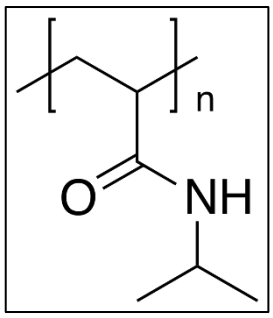

Figure 1) Structure of PNIPAm.

The monomer units of PNIPAm, NIPAm, can be polymerized via free radical polymerization in a homo-polymerization reaction[33]. By copolymerization with poly(ethylene glycol) diacrylate (PEGDA), the PEGDA crosslinks the PNIPAm chains forming a hydrogel. The crosslinking has a limited effect on the hydrophilicity – hydrophobicity switching around the CST, though the thermo-response is affected, becoming kinetically slower than the free polymer transition[34]. The resulting gel is thus swollen (~60 - 70% water) below the CST with hydrated polymer chains. Above the CST, the chains become hydrophobic, transition to the globular state and water is expelled from the gel network. Macroscopically this is seen as shrinking of the gel to

approximately 50% of the original volume[III] [37]. Another commonly used crosslinker is methylene-*bis*-acrylamide.

1.2.2 Functionalization of PNIPAm Gels.

The shrinking-expanding response of PNIPAm gels has already found many uses in applications across a range of fields (see section 1.2.3). For use in robotics, the actuation by shrinking and expanding should be fast and spatially controllable. However, without modifications the shrinking rate is limited by the rate of external heating. This is considerably slow (minutes) due to heat dissipation, and greatly limits the potential applications[35]. Additionally, it is impossible to induce asymmetry in the shrinking of homogenous gels, with external heating[38]. Thus, to overcome these limitations, research has focused on functionalizing PNIPAm gels by incorporation of nanoparticles, electronic circuitry or chemical modification[35,39]. Of relevance to this research is the photothermal conversion achieved using gold nanoparticles.

1.2.2.1 Photothermal Conversion

Light energy can be converted to thermal energy by resonant absorption of photons by nanoparticles[40,41] [IV]. A property of metallic nanoparticles is that the oscillating electric field component of incident light provides an oscillating force on the negatively charged electron cloud, present in all metals. The subsequent oscillation of the electron cloud, a so-called plasmon, exerts its own electric force on the lattice of positive ions. This is a restorative force due to the attraction between the positively charged ions and the negatively charged electron cloud. The system can

---

[III] Different molecular weights of PEGDA oligomers, different crosslinkers as well as different methods of gelation have a direct effect on the swelling ratio [35,36].

[IV] Plasmonic heating is not specifically necessary for the conversion of light to heat – a similar effect can be achieved using carbon black. What is necessary is an extra high extinction coefficient for the light absorption.

then be viewed as an harmonic oscillator which has its own natural frequency, dependent on: electron density and effective mass, and the shape and size of the charge distribution. If the wavelength of the light, incident on a nanoparticle, matches this natural frequency then the nanoparticle is driven to oscillate resonantly and thus with maximum amplitude. The oscillation of the nanoparticle can be seen as the production of thermal energy. By incorporating nanoparticles in the matrix of PNIPAm gels, they can be heated rapidly and locally via this photothermal effect[42]. This research replicates the methods of Sershen et al. (2005) by incorporating spherical gold nanoparticles (diameter = 15 nm) such that 532 nm laser light photothermally heats the gel. The gels produced should have small enough pore sizes such that the nanoparticles are physically trapped within the gel and the number density of the gold particles should not be so great as to cause plasmonic interference between the particles[43]. Such interference would shift the absorption peak of the nanoparticles and may have an effect on the efficiency of photothermal conversion.

1.2.2.2 Alternative Heating Methods

Shape changes in PNIPAm gels have been shown to be programmable by incorporation of an electronic micro-heating circuit. Shape changes are induced by reconfiguration of the gels structure as heated areas shrink[8]. Another method is to produce gels embedded with magnetic nanoparticles. With an oscillating magnetic field, the nanoparticles can be driven to vibrate and heat the gel, similarly to the case of photothermal conversion. This has the benefit of being globally effective within the field and can be used on living tissues[44–46].

1.2.3 Applications of PNIPAm.

The swelling/de-swelling properties of PNIPAm make it ideal for use as actuators and valves. Mechanical work can only be achieved through actuation, by definition it is ‘the fact that makes a machine start to work’[47]. Controllable folding of PNIPAm sheets has been extensively

researched as a route to developing soft actuators and is mostly determined by varying the polymer density within the gels[48–51]. Additionally, the volumetric changes of homogenous gels allow for the opening and closing of valves in microfluidic devices[37]. The force exerted by PNIPAm as it expands, together with its softness has led to its use in single cell deformation analysis[52].

PNIPAm is moderately bio-compatible and has a phase transition temperature close to the temperatures inside a human body (37°C). These properties makes it an ideal candidate for controlled drug delivery[53]. The porosity of the gels allows for the loading of medicines and the de-swelling property allows for controlled release[54]. By functionalizing the gels with gold nano-rods, release of a model drug has been shown to be effective by photothermal heating with a near infra-red (NIR) laser[55] [V] (section 1.2.2.1).

Some other applications of PNIPAm include: cell sheet engineering, purification of water by heavy metal adsorption and bio-sensing[34,54,56,57].

1.3 Microgel Fabrication Techniques

There are a few possibilities available for microgel fabrication techniques for soft, responsive materials. Relevant to this research is *stop-flow lithography* though others will be discussed to provide an overview of the 'state of the art' and to provide a comparison with this research.

1.3.1 Stop-Flow Lithography

Stop-flow lithography is a high throughput microfluidic method for producing polymeric particles of well resolved geometry on the micro-scale[58]. A photo-polymerizable monomer solution

[V] The importance of NIR irradiation is that it can permeate effectively through living tissue.

(henceforth known as pre-gel) flows through a microfluidic channel by compressed air pressure, in fixed intervals of flow and non-flow. The channel is observed under a microscope which can also provide an illumination source through its objective. Whilst the flow is stopped, monochromatic light is then focused on the channel by the objective such that, when pre-gel and wavelength of light are matched, the pre-gel photo-polymerizes in the light. By focusing the light through a photo-mask, the shape of the polymer material produced is given by the mask. After polymerization of a particle (or an array of particles), the flow is switched on to transport the particle(s) and provide space for the process to be repeated. This cycle of 'Stop-Polymerize-Flow' allows for the production of thousands of identical microgel particles per hour of distinct and arbitrary shape. The depth of the particles is given by the depth of the channel and the intensity of the polymerising light. The cross-linking density of the particles is dependent on the intensity of irradiation, duration of irradiation and crosslinker concentration in the pre-gel. SFL has already been used for biomolecular analysis, and the production of multifunctional microgels, barcoded microgels and magnetic microgels, amongst others[59–62].

1.3.2 Alternative Techniques

Alternative techniques for the production of microgels include: micro-moulding, droplet-based microfluidics and, more recently, additive manufacturing. All techniques listed, as with stop-flow lithography, require the matching of hydrogel pre-gel (such as monomer NIPAm) to crosslinking agents (such as PEGDA)[63].

Micro-moulding uses a micropatterned master mould, made usually from glass, PDMS or silicone. The hydrogel pre-gel is loaded in the master and crosslinked. After cross-linking the microgels are removed from the master by washing. The technique can produce gels of distinct shape with dimensions on the order of 1 μm[64]. Combining the technique with pneumatic

microvalves has been shown to produce multi-compartmental gels for bio-engineering[65]. However, the technique is a batch process, which is a limitation compared to the continuous SFL technique used in this research. Droplet-based microfluidics, on the other hand, is a continuous method of production. Droplet formation within microfluidic channels, by directing pre-gel solutions from a channel into a larger microfluidic channel containing a flowing supply of cross-linking agent. The shear forces produce droplets of the pre-cursor which solidify homogenously in the cross-linking solution. The technique can produce picolitre droplets at a rate of hundreds of hertz[66]. The technique is limited compared to SFL by being non-scalable and only droplet shaped gels being produced. Finally, the principle of additive manufacturing (3d printing) has been scaled down to the microscale by using two-photon lithographic techniques[67]. Two-photon lithography allows for highly localised photo-polymerisation in 3d space. By using a two-photon absorbing photo-initiator with the pre-cursor, polymerisation only occurs at the focal point of the laser, the only location where the initiator can simultaneously absorb two-photons. The volume that is polymerised, the voxel, can be resolved to as low as 150 nm[68]. This means hydrogels can be printed from any virtually created 3d designs, at an unprecedented resolution. This is a great advantage over SFL, which can only precisely resolve 2d geometries. The technique is greatly limited by the production rates, compared to SFL. However, it offers the best method for rapidly prototyping microscopic designs[67,69].

2 Materials & Methods

2.1 Chemicals List

Name	Abbreviation
N-iso-polyacrylamide	NIPAM
Poly(ethylene glycol) (Mw = 400 kDa)	PEG
Poly(ethylene glycol) diacrylate (Mw = 700 kDa)	PEGDA
Lithium phenyl-2,4,6-trimethylbenzoylphosphinate	LAP
Trisodium Citrate	Na_3Cit
Tetrachloroaurate trihydrate	H_3AuCl_4
Polydimethylsiloxane (silicone elastomer + curing agent)	PDMS
Methylene-bis-acrylamide	MeAcm
Polyvinylpyrrolidone (Mw = 360 kDa)	PVP
Trimethoxy (octodecyl) silane	
Trichloro (1H1H2H2H-perfluorooctyl) silane	
Sodium Hydroxide	NaOH
Darocur®.	
Tween 20	
Pluoronic	

All chemicals were used as provided.

2.2 Pre-Gel Composition

2.2.1 Gold Nanoparticle Synthesis.

Spherical gold nanoparticles with diameter 15 nm (GNPs) were synthesized using the commonly used citrate method[70]. 300 µL of $HAuCl_4$ (1% w/w) was diluted in 30 mL of MilliQ water in a 30 mL disposable glass vessel and boiled at approx. 100°C[VI] with a stir bar to prevent excessive bubbling. Upon reaching a temperature where a steady stream of bubbles was produced, 600 µL of Na_3Cit (1% w/w) was added in one go and the solution was left to reflux. Within 15 minutes, the solution undergoes colour changes from clear-pale-yellow to black-blue to ruby red.

Upon reaching the ruby red colour, the solution is allowed to cool as this indicates the formation of monodisperse GNPs.

The diameter of the GNPs was verified using UV-vis spectroscopy (peak at ~530 nm equating to 15 nm GNPs). The number density was calculated to be 1.70×10^{18} m^{-3} (Appendix 1). The solution was stable enough to be kept at room temperature in the dark for up to two weeks[VII].

2.2.2 Concentration and Stabilisation of Gold Nanoparticles.

Firstly, the ~30 mL of GNP suspension was centrifuged at 15,000 g for 30 mins in a polypropylene 50 mL centrifuge tube (Beckman Coulter) and in an Avanti J-20 XP (Beckman Coulter) centrifuge**.** The supernatant was discarded and ~1.6 mL of the concentrated gold solution was divided into two microcentrifugation tubes. To stabilise the sample, 0.3 mL of PVP (10% w/w) was then added to each tube and they were sonicated for 20 mins in the bath before being left to stand for 30 mins. This was to allow proper equilibration of the PVP with the GNPs, sterically stabilising them. The tubes were then centrifuged at 15,000 g for 2 hours, after which, the supernatant was discarded and the concentrates were combined to give a total volume 100 µL - 125 µL.

At this concentration the number density is calculated to be 5.10×10^{20} m^{-3} (Appendix 1). The sample was not expected to be stable enough to be stored and so was always used within a few hours.

2.2.3 Final Composition.

37 mg of NIPAm, 20 mg PEGDA and 1.5 mg of LAP were added to 100 µL of the concentrated GNPs (described in 2.2.2) in a microcentrifugation 1.5 mL tube. The tube was then

---

[VII] The stability of the colloid may extend to well beyond two weeks though this claim comes only from qualitative inspection of a samples colour months after the synthesis.

wrapped in foil to prevent premature photo-polymerisation, and was sonicated for 5-10 mins to maximise dissolution of the solutes. Before use in stop-flow lithography, the sample was centrifuged at 5000 g for 2 mins to sediment any dirt or gold agglomerates. This composition, hence-forth referred to as 'pre-gel', was highly light-sensitive and so was always used directly after production.

2.2.4 Increasing the Sensitivity of the Gel.

The pre-gel composition was modified by decreasing the PEGDA content and replacing it with non-crosslinking polyethylene glycol (PEG) (Mw = 400 kDn) and the crosslinker methylene-bis-acrylamide (MeAcm). The pre-gel was made in the same fashion as previously described, with 100 µL gold colloid, and the mixing ratios can be seen in table 1. Circular disk particles (photomask G, section 2.6) were made using the different mixtures and following the standard SFL procedure. The shrinking response of the gels produced was measured by heating a sample of the gel disks in a capillary and measuring the change in diameter as a function of temperature (Appendix 4). The temperature was raised from 25°C to 75°C and then cooled back down at a rate of 2°C per minute. The diameter was measured in ImageJ and normalised to the initial diameter at 25°C.

Table 1

Mix	PNIPAm (mg)	PEG (mg)	PEGDA (mg)	MeAcm (mg)	LAP (mg)
1	37	20	0	2	1.5
2	37	18	2	2	1.5
3	37	15	5	2	1.5
4	37	10	10	2	1.5
5	37	5	15	2	1.5

2.3 Stop-Flow Lithography

Protocols for stop-flow lithography (SFL) are replications and adaptations of those described by Dendukuri et al. (2007)[58]. All operations with open solutions or exposed channels

were performed in a laminar flow cupboard to prevent dust contamination and materials were transported in cleaned petri dishes. Additionally, Nitrile or Latex gloves were worn, washed sequentially with detergent, ethanol and MilliQ water and then dried with clean air. After this, contact by the gloves with anything that had not been cleaned was strictly avoided.

2.3.1 Production of Microfluidic Channels.

2.3.1.1 Preparation of PDMS mixture.

To make the PDMS mixture, 35 g of the silicone elastomer was added to 5 g of curing agent in a 50 mL centrifugation tube. The mixture was homogenised until opaque grey and centrifuged at 15,000g for 15 minutes to sediment dust and remove bubbles. At room temperature the mixture began to cure and so was used within hours of production.

2.3.1.2 Preparation of Silicon Wafer Template.

A silicon wafer patterned by SU-8 photoresist with positive relief channels was used to template the PDMS. The channels had a height of 30 µm and width 200 or 400 µm. The wafer was fixed on the base of a petri dish with PDMS. Before use in moulding, the wafer was washed with isopropanol followed by MilliQ water and then dried. After every 10 usages the surface was silanised by vapour deposition of 1H1H2H2H-perfluorooctyltrichlorosilane.

2.3.1.3 Production of Microfluidic Channels.

The PDMS mixture produced in 2.3.1.1 was poured over the silicon wafer from the corner and with care taken to avoid folding (layering of mixture) as this produces pockets of air in the fluid. When a depth of 0.8 - 1 cm was reached, the dish containing the wafer was placed in a vacuum desiccator which was then evacuated with a membrane pump in order to remove any remaining air trapped in the fluid. After the formation of bubbles on the surface of the PDMS, the desiccator valve was closed. After disassembly with the pump, the valve was placed such that the

opening faced the laminar flow source and opened to ensure that only dust-free air re-entered the chamber. The petri dish lid was then cleaned and placed back on the mould after which the dish was left in an oven at 65°C overnight.

After curing overnight, the PDMS was cut with a razor around the edges of the silicon wafer with care taken to ensure minimal scratching or other damages to the wafer. The piece of PDMS could then be peeled from the silicon surface and placed with the channels face up in a clean petri dish[VIII]. Scotch tape was then stuck over the channels on the PDMS, parallel to the channels and such that only one layer covered them. The PDMS was then cut into smaller pieces (chips) with only one channel in each and with sufficient space around the channel (~1 cm total width, ~4 cm total length). Inlet and outlet holes were then punctured through the PDMS from the taped side using a biopsy needle. The inlet hole was punctured through one of the circular inlets at either end of the channel. The outlet hole was punctured through the channel itself to allow larger particles to be produced in SFL. The tape was then removed from the chips and they were washed briefly with ethanol and MilliQ water and dried. They were then placed, channel down and gently, on the partially cured PDMS-glass slides (produced in section 2.3.1.4) such that full contact was made between the slide and the chip. The chips were then left in the oven overnight at 70°C. In the case that more than one chip was bound to one slide, they were separated by cutting the slide with a diamond-tipped pen. Inlet and outlet channels were made by making capillaries by cutting a 0.8 mm syringe needle. The inlet capillary was cut with the Luer adapter remaining to allow connection to the compressed air flow and loading of pre-gel. The outlet was a cut from the middle of the needle and was bent such that the 'out' end was facing down. The metal ends of the

[VIII] Extreme emphasis on clean in the present environment.

capillaries were filed down to give a circular cross-section and flat end to prevent damage to the PDMS. (See Appendix 5 for photographs)

2.3.1.4 Spin-Coating PDMS on Glass Slides.

20 g of silicone elastomer was added to 2 g of curing agent, homogenized and centrifuged in the same procedure as 2.3.1.1, the only difference being the elastomer to curing agent ratio.

Glass slides were washed by sonication in 1 M NaOH, rinsed with MilliQ water and then dried with the clean air gun. They were then attached in the homemade spin-coater. 1 mL of the PDMS mixture was then syringed onto the slide, lengthways along the middle. The slide was then spin coated at 2000 rpm for 1 minute after which the slide was removed and placed flat in a petri dish.

After spin-coating the desired amount of slides, they were placed in the oven at 70°C for a length of time depending on the desired use. For use in microfluidic channels (2.3.1.3), they were left in the oven for 35 mins to allow partial curing. For use in wells (2.4.2.1), they were left overnight to be fully cured.

2.3.2 Microscope Set-Up.

A Nikon Ti-U inverted microscope was used for SFL, observation and operation of the microgel crawlers. Nikon NIS software was used for operation. A Nikon Intensilight™ Hg lamp ($\lambda < 405$ nm) was used to provide the illumination through the objective for photo-crosslinking. The duration of illumination was controllable via NIS. During SFL a 480 nm long-pass filter was placed over the condenser to prevent crosslinking from the diascopic light-source. Compressed air was used to pump liquid through the channel and controlled using a pressure gauge. A three-way solenoid valve connected the air flow to the computer to allow rapid switching between operating

and atmospheric pressure (flow and non-flow) via NIS. Photomasks could be placed in a custom built holder, positioning them in the focal plane of the objective. Focus could be achieved by controlling the objective to channel distance. (See Appendix 5 for photographs)

2.3.3 SFL Procedure.

Firstly, the channels were always washed sequentially with ethanol, water and then tween 20 (0.5% w/w). A PCR tube with two 1.5 mm holes bored in the cap was filled with 150 µL tween 20 (0.5% w/w) and connected to the outlet capillary through one hole such that the end of the capillary was submerged. The other hole served to release pressure as liquid was pumped into the PCR tube. After checking the channel was clear of large pieces of dirt, 50 µL of pre-gel was loaded into the female Luer connector of the inlet needle. The pre-gel was then pumped through the channel manually using a 1 mL syringe until it visibly flowed through the chip and into the PCR tube. The compressed air source was then connected and the chip was placed on the microscope stage. To prevent premature photo-polymerisation, an opaque plastic barrier was constructed around the chip to keep it in darkness. With a 40X objective, the edges of the channel were found and used as a simple visual reference for focussing. The solenoid valve for switching the fluid flow and the shutter for switching the UV illumination were then controlled by NIS in the following manner: 1) Flow: valve open, shutter closed, 0.3 s; 2) Stop: valve closed, shutter closed, 0.2 s; 3) Print: valve closed, shutter open, 0.05 s. The three operations were set to cycle indefinitely. To increase the spacing between the polymerised gels, the pressure was increased gradually. To prevent excessive wastage of the pre-gel, the pressure was decreased gradually. Ideally, an interparticle distance of 50 µm was maintained and was achieved with around 0.5 psi. The definition of the gels, given by the focus of the UV light, was controlled using the focussing knob of the objective lens. After production of the desired number of particles, typically 5000-10,000

from a full 50 μL, the channel was purged and washed by manually pumping a small amount of Tween 20 (0.5% w/w) through the channel. The dispersion of microgels collected in the PCR tube were then washed in a cycle of 1) Disturbing the dispersion; 2) Sedimentation (~5 mins); 3) Removal of most of the liquid, leaving the sediment submerged, and replacement with tween 20 (0.5% w/w). The cycle was repeated at least 4 times to ensure the minimum amount of pre-gel was left in the dispersion. The dispersion was then transferred to a new and clean PCR tube and could be stored in the fridge for months as the tween prevented sticking between the particles.

2.4 Observation and Control of Microgel Crawlers

2.4.1 Operation of Laser.

A 200 mW diode laser (λ = 532 nm) was placed in the condenser lens of the microscope to provide stationary positioning and controllable focus. As such, the diascopic illumination that would have come through the condenser was replaced by fitting four white light LEDs around the laser (~0.5 W). With the laser stationary, the XY stage was moved via NIS. This is equivalent to moving the laser over the sample and shall henceforth be referred to as such. A 536 nm long-pass filter was placed between the sample and the objective and a RITC cube (Semrock) were both used to protect the microscope. The laser intensity could be lowered by attaching a 12 mm filter to the end of the laser (OD; 0.3, 0.5, 0.6 or 0.9)[IX]. The duration of laser pulses was controlled using a built-in-lab relay circuit or by the NIS software. (See Appendix 5 for photographs).

[IX] The OD filter was selected such that the illumination intensity was sufficient to achieve actuation whilst simultaneously preventing damage from too high intensity. 0.5 and 0.6 were used for experiments described in this research and the differences between them were not deemed to significantly alter the results.

2.4.2 Modifying the Crawling Substrate.

Wells used to observe a sample of the microgels were built by fixing either circular washer rings (1.5 cm) to the surface, or by cutting the top piece of a microcentrifugation tube and fixing this to the surface. In both cases, the same PDMS mixture as prepared in section 2.3.1.1 was used as a glue, after-which, the well was left to cure in an oven at 70°C overnight. (See Appendix 5 for photographs).

2.4.2.1 PDMS Surface.

The fully cured PDMS slides as described in section 2.3.1.4 were used as the surfaces for wells. They were cleaned after use by rinsing with ethanol and water and then dried with a stream of air.

2.4.2.2 Perfluorinated Surface.

20 µL of trichloro (1H1H2H2H-perfluorooctyl) silane was added to 300 µL of MeCN in a 1 mL glass vial. Glass slides were washed in 2 M NaOH solution by sonication and then rinsed with MilliQ before drying with clean air. The mixture was then deposited on the surface via vacuum vapour deposition as follows. The glass vial containing the mixture was placed in a desiccator with the glass slides. The desiccator was then evacuated with a membrane pump and left for 15 minutes, after which, the desiccator was opened and the slides were stored in the laminar flow cupboard.

2.4.2.3 Octadecyl Modified Surface.

10 µL of Trimethoxy (octadecyl) silane was added to a mixture of 400 µL of MeCN and 10 µL of Et_3N in a 1 mL glass vial. The same procedure as in 2.4.2.2 was followed but with this new mixture.

2.5 Summary of Experiments

2.5.1 Investigating Potential Crawling Mechanisms.

2.5.1.1 Ratcheted Crawlers.

Firstly, crawling with ratcheted microgels on PDMS surfaces (2.4.2.1) was attempted by using photomasks L and M. The crawlers were irradiated with laser pulses of 0.5 s ON and 0.5 s OFF. The pulses were directed in the centre of the gels in order to actuate as much of the gel as possible.

2.5.1.2 Off-Centre Actuation.

The particles were irradiated to actuate for various lengths of time and in various positions on the gel until a crawling mechanism was clearly observable. It is necessary to state now that off-centre irradiation of particles of arbitrary shape with laser pulses of 0.5 s ON and ≥ 0.5 s OFF led to a net displacement of the particles. Repeated off-centre actuation led to a controllable directed motion of the particles. The mechanism leading to such displacement was unclear at this stage and became the principle focus of the research project.

2.5.1.3 Peristaltic Motion.

Peristaltic motion was attempted by moving the laser in one direction over the length of particles produced with photomasks D and L with the beam constantly ON. The laser was turned OFF and moved to the original position and the process was repeated.

2.5.2 Determination of the Principle Mechanism.

2.5.2.1 Crawling on Different Surfaces.

Crawling by off-centre actuation (2.5.1.2) was attempted on the PDMS, glass, perfluorinated and the octadecyl brush surfaces (all in MilliQ water). The average step-sizes can be found in table 3.

2.5.2.2 Measuring Changes in Friction During the Shrinking-Expanding Cycle.

The inner surface of a glass capillary (50x5x0.5 mm) was spin-coated at 2000 rpm for 1 minute with PDMS (elastomer : curing agent : toluene = 10:1:10 volume ratio). Circular disk particles (diameter = 115 μm, photomask G) were inserted in the capillary in a 0.5% w/w tween 20 solution. The capillary was sealed with UV glue and was bound to a heating stage attached to the stage of a 90° tilted microscope, such that the particles were visible side-on through the side of the capillary (50x0.5 mm) (2.5.5.B). The capillary was tilted to 10° to induce sliding of the crawlers. The stage was then heated from 25°C to 65°C and back at a rate of 20°C per minute. The diameter of the disks, velocity of the sliding disks and temperature were obtained from microscopic observation.

2.5.3 Investigating the Mechanism.

2.5.3.1 Measuring Step Size as a Function of Irradiation Position and Length of Crawler.

Crawlers of equal width and varying length were synthesised (photomask A, B and E). They were then irradiated with pulses of laser ON: 0.5 s and OFF: 0.75 s. The irradiation was aimed in the centre, width-wise, of the particle and at various positions along the length of the crawler. The crawling was recorded with NIS and the net displacement, total change in length (ΔL) and the displacement of the front edge (step back) were measured in ImageJ (2.5.5.A).

2.5.3.2 Surfactants.

The step sizes of 100 μm x 50 μm crawlers on a PDMS surface were measured in different concentrations of surfactant Tween 20, shown in table 2. The same sample of crawlers was used for the tween 20 and so the concentration was only ever increased. A fresh sample of crawlers was used for the Pluoronic tests. To remove dust, the solutions used were filtered using 0.2 μm filters before use.

2.5.3.3 Crawling Uphill.

The step sizes of 100x50 µm crawlers were measured as they crawled uphill on a tilted PDMS surface. Laser pulses were set to ON: 0.5 s and OFF: 0.75 s (2.5.5.D).

2.5.4 Steerable Crawling and Micro-manipulation.

Crawlers were synthesised using photomask K and observed to crawl on a PDMS surface. Laser pulses (ON: 0.5 s; OFF: 0.75 s) were directed at the open ends of the gel in order to drive a tank-like crawling mechanism. Alternating which sides were irradiated resulted in forward crawling (2.5.5.C). A crawler was steered to navigate between pieces of dirt over a total length of approximately 5 mm. PEGDA cubes (25 µm x 25 µm x 25 µm) were synthesized by SFL using photomask J and a pre-gel composition of 0.5 mL PEGDA and 100 µL Darocur®. The blocks were pushed using the front end of the steerable crawlers.

2.5.5 Experiment Figures

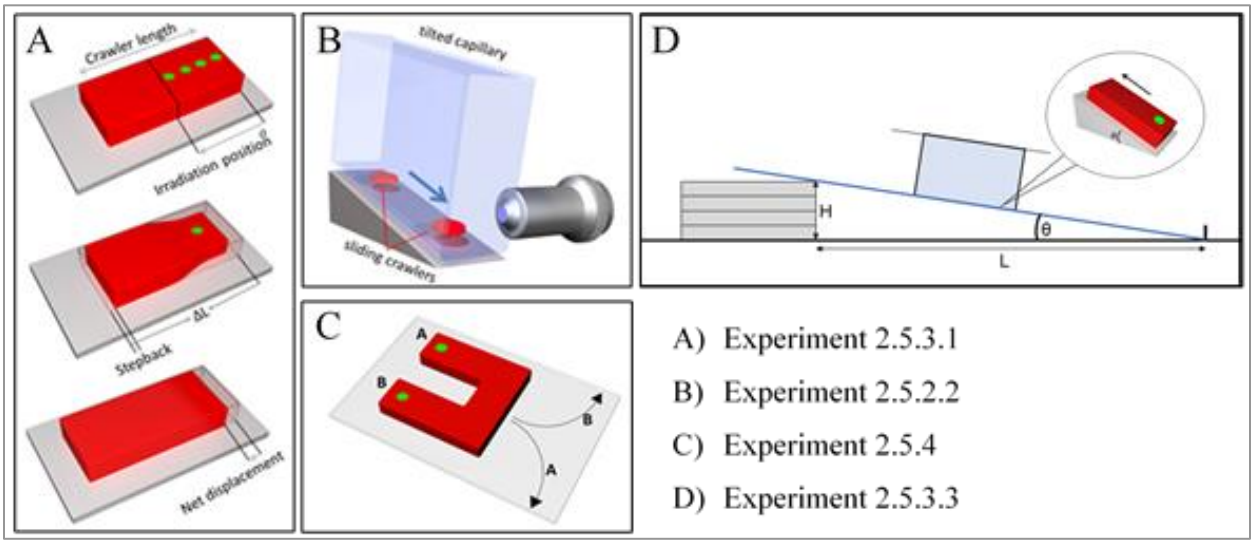

2.6 Photomasks

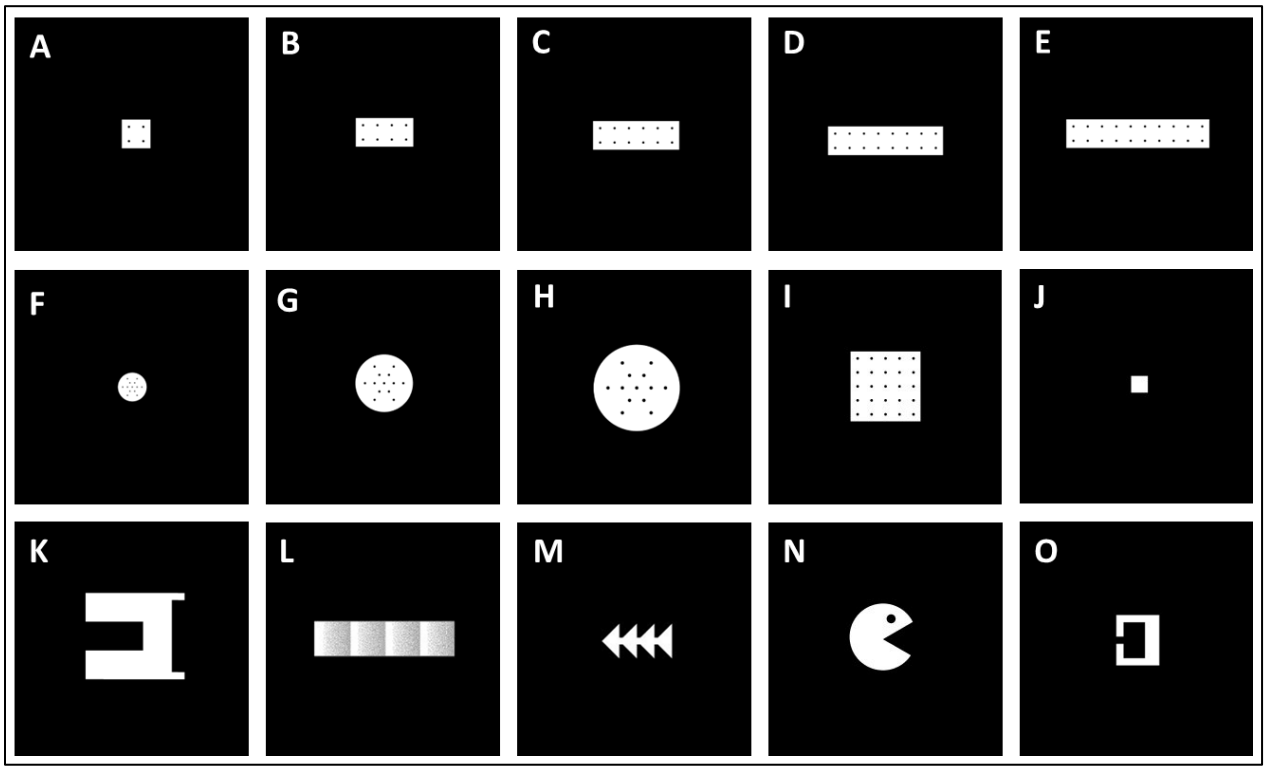

Photomasks were designed in Autodesk AutoCAD 2017 and printed with a resolution of 36,000 DPI. The black dots on the masks were used as reference points for particle tracking and to improve accuracy when aiming the laser. They had no effect on the crawling mechanism. All masks are equivalently scaled and photomask A produces 50 μm x 50 μm microgels by illumination through a 40X objective.

3 Results and Discussion

3.1 Synthesis and Review of Methods

The SFL technique works as desired and described in sections 1.3.1 and 2.3. The method allows for the production of roughly 6000 microgels in one hour, though this could be increased with simple modifications to the procedure. One such modification is to include a stage movement operation during the 'print' step of the procedure. After producing a particle, the stage is repositioned to produce another particle or particles. This could be performed multiple times before the 'flow' step and allows for the polymerisation of more pre-gel, and thus more particles, in each full cycle. Some problems were encountered in SFL though solutions were easily found. Some microgels become stuck in the channel after polymerisation, mostly due to excessive cross-linking. This is solved by always washing the channel with Tween 20 before use as well as using lower polymerisation light intensities. Another problem is maintaining equilibrium of the liquid pressure during the 'stop' stage. Backflow through the channel occurred regularly and could be prevented by opening the PCR tube with the outlet needle attached. This allows the pressure to equilibrate and prevent backflow.

The gels produced are shown to actuate effectively by irradiation with the laser. Effectively here referring to a quick transition from swollen to fully shrunk, on the order of 100s of milliseconds. The focussing of the laser is crucial to achieving effective actuation. With too small a point of irradiation, that is to say when the focal point of the laser is within or near the gel (figure 2A), the heating of the particles is rapid and to temperatures sufficient to destroy the gel. This is by the production of steam bubbles which tear the gel from within. With too great a point of irradiation (figure 2B), the microgels are barely responsive and shrink homogenously to some 95%

of their original volume. To prevent burning, whilst maintaining localised heating, the 0.5 & 0.6 OD filters are used with the laser.

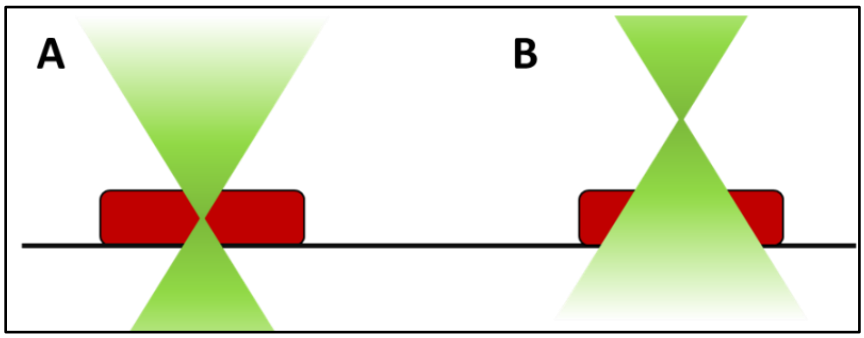

Figure 2) A) Focal point of the laser is within the gel, causing burning. B) Irradiation point on the gel is too wide and the photothermal effect is diminished.

The crosslinking density of the gel means the GNPs are permanently trapped in the microgels, observed by their continuously effective actuation with the laser, up to months after their production. The number density of the GNPs in the hydrogel is assumed to be the same as in the final concentrated pre-gel solution: $5.10 \times 10^{20}\ m^{-3}$. This means the average interparticle distance between the GNPs varies between 1100 nm and 550 nm in the swollen and shrunken states respectively. These distances are sufficiently long that interparticle interference effects would be neglected and, indeed, are not observed. (Appendix 1).

A regularly occurring problem is dust contamination in the samples, though this was constantly improved over the course of the project. One effective technique to reduce the amount of dust is to produce a maximum number of microgels in each SFL synthesis – approximately 10,000 for each shape. By then adding a smaller volume of the suspension of these gels to the solutions in the well, the number of contaminants arising from the SFL procedure is greatly reduced. This is thought to be the greatest source of contaminants as it could also include unintentionally polymerised gel fragments or undissolved solids from the pre-gel mixture.

3.2 Discovery of the Crawling Mechanism

From the experiments described in section 2.5.1, it is found that off-centred actuation of the microgels, on a PDMS surface, results in a net displacement of the gel (figure 3). Repeated actuation leads to a crawling mechanism which shall henceforth be referred to as the 'principle mechanism'.

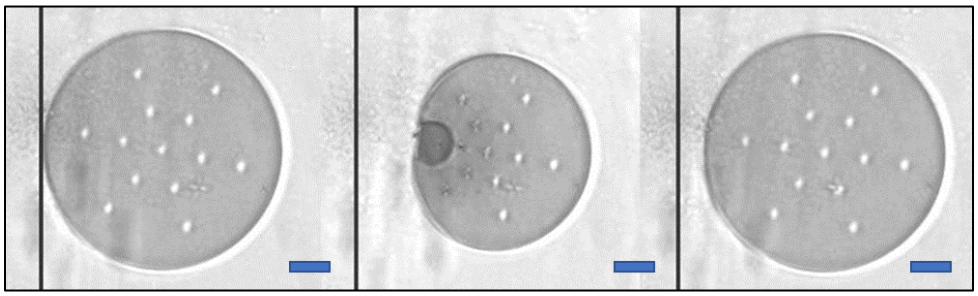

Figure 3) The principle mechanism demonstrated on a circular, 100 µm diameter crawler. Scale bar = 12.5 µm.

The principle mechanism is shown to be effective for a various crawlers shapes and sizes. Shapes shown to crawl via off-centred actuation are those produced with photomasks; B, C, D, E, G, K, L, M & N, which shows an independence on particle shape. The size of the particle imposes limits on the effectiveness of the principle crawling mechanism. Photomasks A and F (50 µm x 50 µm square and 50 µm diameter circle) produce particles that are too small to be actuated asymmetrically due to heat dissipation through the gel and the lower limit of the beams focus when avoiding burning. It can be said that the minimum amount of gel that is completely shrunk by the laser is an area of approximately 25 µm x 25 µm of the swollen gel. This can also be seen in figure 4, where the swollen and shrunken areas of a 220 µm x 50 µm gel are both visible. The completely contracted area shows a darker phase contrast than the rest of the gel.

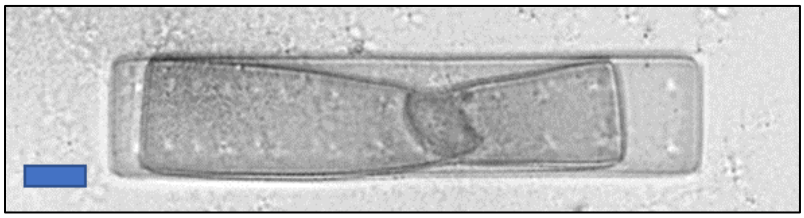

Figure 4) Overlay of a 220µm x 50 µm crawler in maximally shrunken and expanded states, scale bar = 25 µm.

The rate of heat dissipation in the gel is non-linear - as the irradiated area of the gel shrinks, it pulls in more surrounding gel which is in turn shrunk by the laser and pulls in more material. Heat also dissipates from the edges of the irradiated sections and further shrinks the surrounding gel. A saturation point is reached when the area of completely shrunken gel is roughly equal to the irradiation area, though this is difficult to quantify as the beam intensity likely follows a gaussian distribution. Further from the irradiation centre, the degree of shrinking decreases radially to zero over a length of approximately 30 µm from the edge of the completely contracted area. Large squares (125 µm x 125 µm) and circles (diameter = 150 µm) (photomasks H & I) do not crawl effectively due to a combination of buckling and excessive weight. The buckling effect arises as the particles become much larger in two dimensions than the third, such that shrinking or expanding induces a stress[71]. The buckling property is observed frequently on particles with both x and y dimension longer than 100 µm and is rarely observed on the various lengths of 50 µm wide particles. This indicates that there is a saturation point at which enough material is shrunken to provide a stress which causes instabilities in the gels 3d shape. The additional limitation of larger particles is that the actuating force provided by the shrinking and expanding cannot push the greater volume of swollen gel during each step.

From these observations it was decided that the 50 µm x 100 µm crawlers (photomask B) would be best suited for further experimentation as they rarely buckle, simplify the investigation

of the mechanism by restricting the off-centre actuation to only one dimension (length) of the crawlers, and minimise the mass that would be pushed in each cycle. Additionally, they are shown to crawl with the largest step sizes, up to 18 µm on PDMS (figure 8). As will be seen, throughout this research there is inconsistency in the step-sizes of the 50 µm x 100 µm crawlers between experiments and with the crawlers in seemingly the same conditions. This is addressed as an additional discussion point in section 5.5. However, any comparisons relating to the step-sizes are in experiments with crawlers from the same sample and with consistent step-sizes and so conclusions drawn from the experiments remain valid.

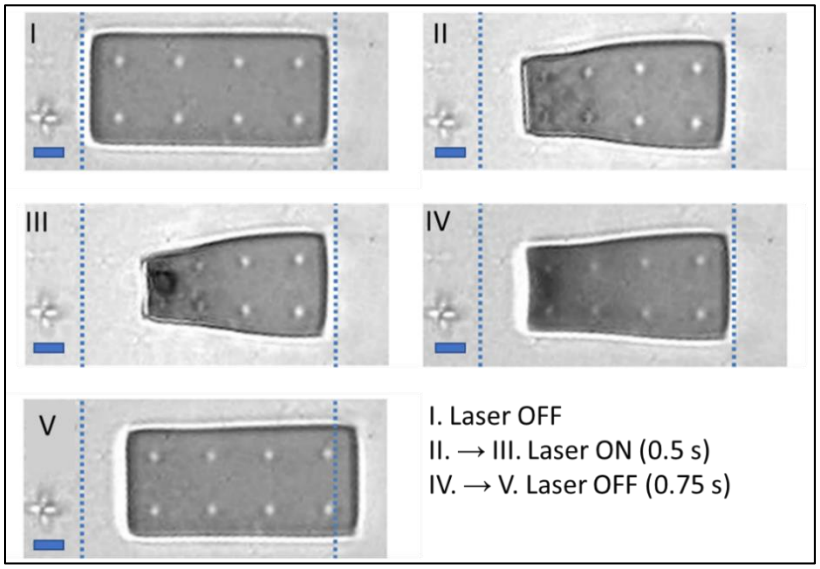

Figure 5) The principle crawling mechanism demonstrated on a 100 µm x 50 µm crawler, scale bar = 12.5 µm.

By observing the principle mechanism in slow motion, it can be divided into individual steps. These are highlighted in figure 5. As one side is irradiated and shrinks, it slides towards the centre of the particle whilst the non-actuating side doesn't change position. Upon switching off the irradiation, the shrunken side of the particle expands and slides along the surface until it reaches a

certain volume at which point it sticks to the surface. The remaining expansion of the gel then drives the non-actuating side forwards.

Table 2) Step-Sizes of 100 µm x 50 µm crawlers in various Tween 20 concentrations.

Tween Concentration (% w/w)	Average Step-Size (µm)
0	4.5
0.05	3.2
0.1	2.7
0.2	8.1
0.5	9.9
1	2.7
2	0

Table 3) Step-Sizes of 100 µm x 50µm crawlers on various surfaces in MilliQ water.

Surface	Average Step-Size (µm)
Glass	3.9
PDMS	5.8
Perfluorinated	0
Octadecyl Modified	4

Varying the concentration and type of surfactant has a significant effect on the efficiency of the crawling. It can be seen from table 2 that both too low and too high surfactant concentrations have a reductive effect on the step sizes. In the case of lowering the surfactant concentration, it is thought that the forces of adhesion between the swollen, non-actuating side of the gel and the substrate begin to exceed to the force provided by the expanding actuating side. Additionally, attempting to crawl in a 5% w/w Pluoronic solution as well as higher tween concentrations, is unsuccessful as the actuating sections of the crawler expand back to their original positions, sliding easily over the surface. It was also easy to observe the sticking or sliding of the gels on the surface

as the laser produced convection in wells. In the low friction Pluoronic samples, the gels slid over the surface in response only to the convection in the sample.

In water, the crawling is most efficient on PDMS surfaces (5.8 μm steps), but is also demonstrated on octadecyl modified and cleaned glass surfaces, though the step sizes are lower (3.9 μm and 4 μm respectively) (table 3). The gels attach permanently to perfluorinated surfaces and could not crawl.

Why the expanding side of the crawlers stick to the surface during the principle mechanism crawling was unclear at this point in the project. Any hydrodynamic forces are neglected as viscous forces completely dominate this system (see section 1.1.3). From the results of the experiments with surfaces and surfactants, it is clear that the friction between the PNIPAm gel and the substrate plays an important role[X]. This was the motivation for the experiment described in 2.5.2.2 for which the results are described in the following section.

3.3 Investigating the Mechanism

Observation of disc shaped crawlers, sliding down a tilted plane during heating and cooling cycles (experiment 2.5.2.2) reveals a hysteresis in the sliding velocities. The measurements of temperature, diameter and sliding velocity show that the sliding velocity of PNIPAm gels not only depends on the temperature/relative size (swelling state) but also on whether the gel is heating/shrinking or cooling/swelling. Figure 6.A shows how when the gel is heated and thus shrinks, it slides at an increased velocity than in its swollen state. Upon shrinking to 70% of its swollen volume and further to 60%, it slides with a constant velocity. Upon cooling of the gel and

[X] The change of wording from adhesion to friction comes by the statement that the friction forces acting on the gel arise from the adhesion forces between the polymers in the gel and the substrate.

subsequent swelling, it decelerates until it reaches a stand-still at approximately 80% of its swollen volume. By plotting the normalised velocities against the swelling state of the gels, it is clear that there is a hysteresis in the sliding velocity of the gels which is dependent on whether the gel is being cooled or heated (figure 6.A).

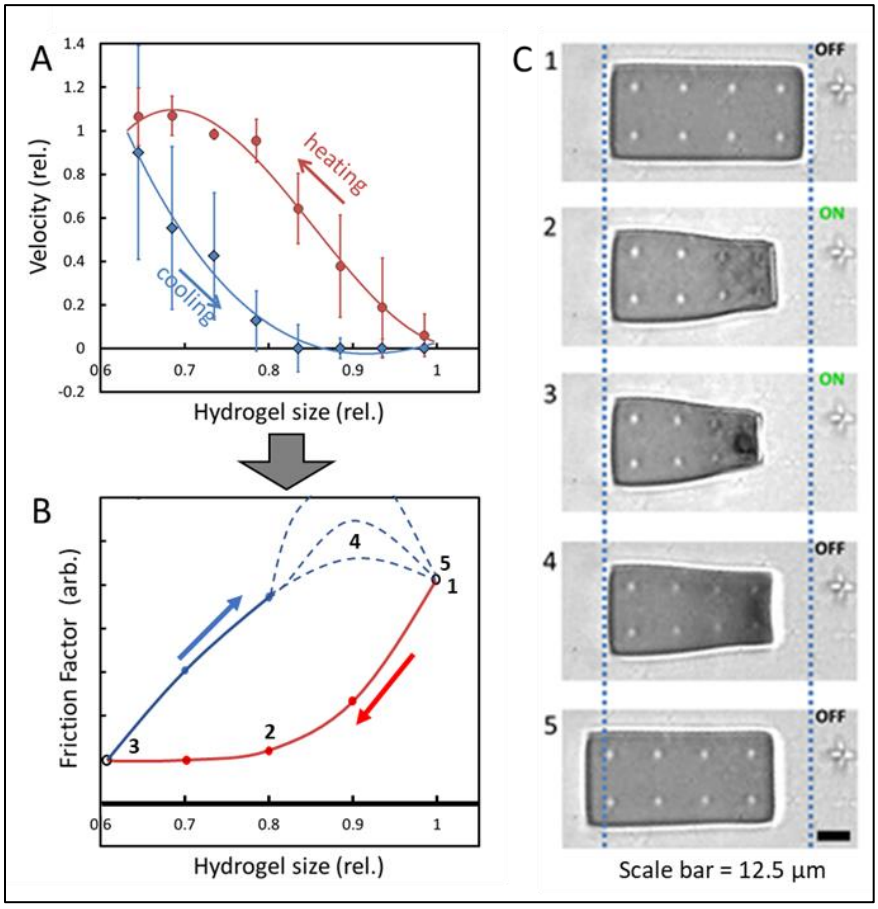

Figure 6) A) Plot of averaged and normalized velocities vs. swelling state of the gel.

B) Approximation of the friction hysteresis with respect to the swelling state of the actuating gel during heating and cooling cycles.

C) The principle mechanism with numbers corresponding to the states labelled in (B).

The sliding velocity can be correlated to the friction between the surfaces as follows:

The friction force ,$F_{friction}$, acting on the gel is equal to the normal force, F_N, of the gel multiplied by the friction coefficient, μ.

(i) $F_{friction} = F_N . \mu$,

The normal force is the product of the gels buoyant mass, *m*, the gravitational constant, *g,* and the angle of the tilted capillary, *θ.*

(ii) $F_N = m . g . cos\theta$

The friction coefficient is proportional to the sliding velocity and a velocity independent friction factor, *k.* This friction factor is dependent on the inter-surface properties of the two materials.

(iii) $\mu = k \cdot v$

When the gels slide with a constant velocity, the friction force on the gel balances with the lateral force, F_l, exerted on the particle by gravity.

(iv) $F_l = F_{friction}$

The lateral force is the product of the gels buoyant mass, the gravitational constant and the angle of the tilted capillary.

(v) $F_l = m \cdot g \cdot sin\theta$

Rewriting equation (i) using (ii) and (iii):

(vi) $F_{friction} = m . g . cos\theta . k . v$

Finally by combining (v) with (vi) by use of (iv), it is shown that the sliding velocity is inversely proportional to the velocity independent friction factor:

(vii) $v = \frac{tan\theta}{k}$

The hysteresis observed in the sliding velocities can then be attributed to a hysteresis in the velocity-independent friction factor between the gel and the surface. A hypothetical plot of the friction hysteresis can then be drawn and is shown in figure 6.B. As the hydrogels decelerate to a standstill, it is impossible to take an accurate measurement of the enhanced friction factor. All that

can be derived is the minimum frictional 'stopping' force that overcomes the lateral 'sliding' force. How much the friction factor is enhanced beyond this stopping point remains unknown and is subject to further investigation[XI].

The hysteresis in the friction factor provides a robust explanation for the principle mechanism. As the actuating side of the particle shrinks, its friction with the surface decreases and so this side slides easily towards the centre of the particle. The other side remains stationary with its unchanged, and greater, friction. As the actuating side then expands, its friction with the surface increases until it is greater than the unchanged friction of the other side. At this point, the expansion of the gel drives the non-actuating side forwards as the resistive friction force is now lower on this side than the actuating side (figure 6.C).

The mechanism described above is the first demonstration of such a frictional hysteresis of swelling and collapsing PNIPAm. Whilst instances of PNIPAm being used to switch friction can be found, they all describe the difference in friction between the collapsed and swollen states and make no mention on the differences between the collapsing and swelling intermediate states[72]. Yu et. al.[73] report on a hysteresis in the adhesion of an AFM tip to a PNIPAm brush surface as the tip is brought to and retracted from the brush, though, this does not match our system. It is thought that the hysteresis responsible for the crawling mechanism originates from the different kinetic paths that the PNIPAm chains undergo as they transition either from globular to expanded states and vice versa[74,75,77]. It has been shown that new hydrogen bonds are formed when the PNIPAm is in the globular/shrunken state. These present an energetic barrier upon cooling that is not present

[XI] Attempts to measure the frictional forces during the shrinking-expanding cycle by use of an atomic force microscope in shear mode were unsuccessful and have been postponed. Such measurements may provide an experimental realisation of figure 6.B.

in heating[76]. As such, there is a hysteresis in the conformation of the polymers, including chains at the surface, as they are being heated or cooled, depicted in figure 7[74]. Nanoscopic differences in the conformation of the PNIPAm chains at the surface alter the surface topology. This may have a large effect on the macroscopic properties of the gels, namely, friction forces between PNIPAm gels and a substrate. It is hypothesised that these forces, and how they change depending on the swelling state, are what determines the hysteresis in the previously discussed velocity independent friction factor.

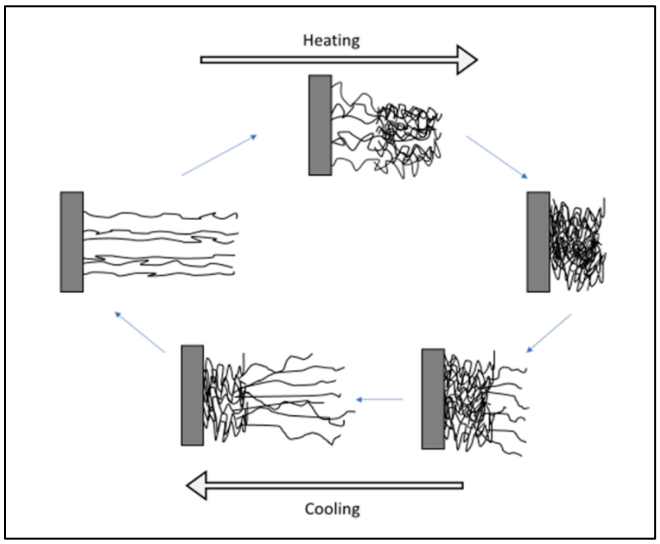

Figure 7) Conformation changes of PNIPAm chains during heating and cooling cycles. Adapted from Liu et. al., (2005)

An understanding of the hysteresis can open up new channels of research as it provides a new method for modulating friction with an extra degree of freedom. One such application is demonstrated in this research by the crawling mechanism. By combining the actuation of the PNIPAm gel with a spatiotemporal control of friction to the substrate, a novel method for crawling by reciprocal actuation has been shown. Another application could be in the development of

artificial muscles, where mediating the friction and contractions of large groups of micro-actuators could yield a macroscopic muscle like response, biomimetic of the sliding between muscle fibres[76].

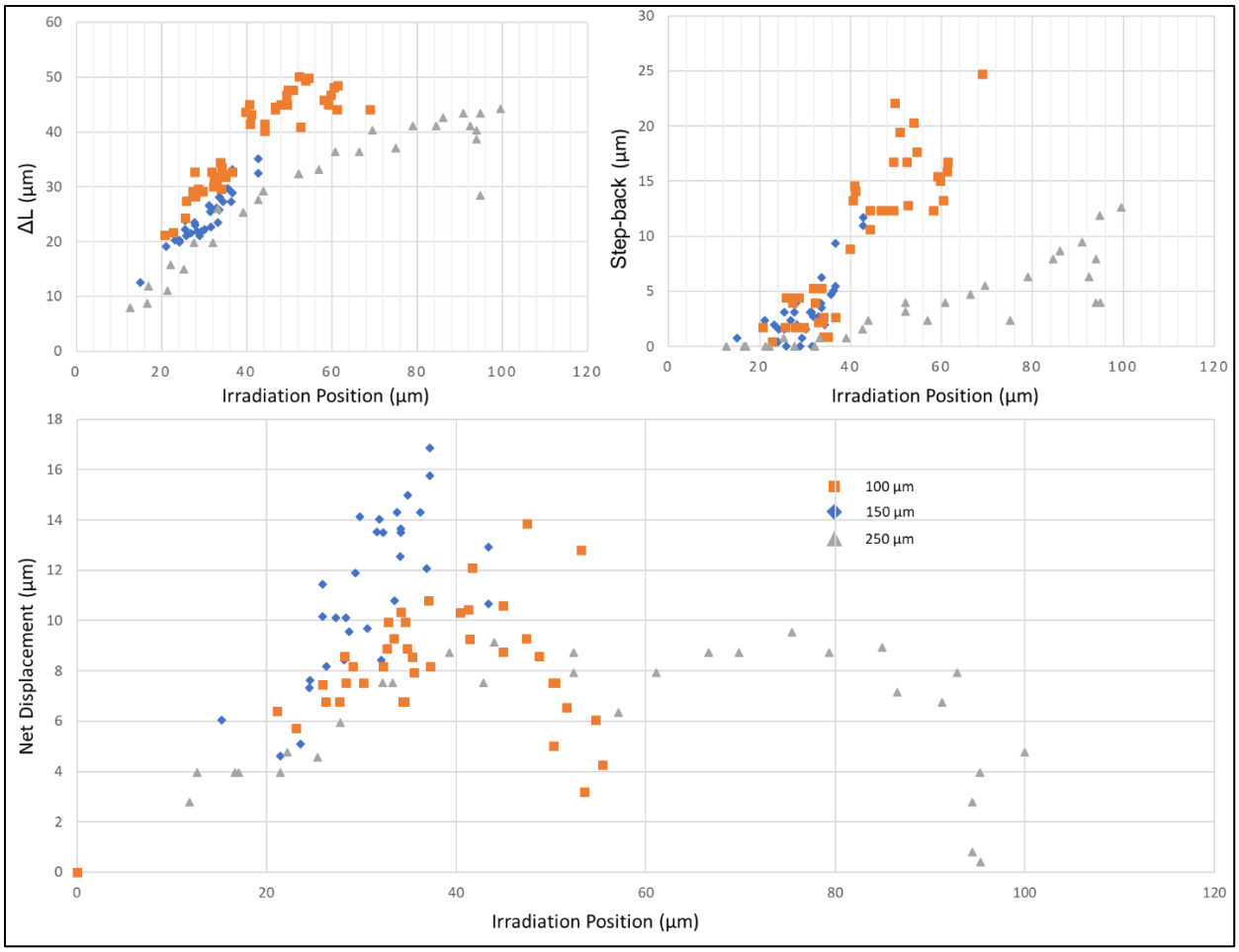

Figure 8) Plots of Contraction (ΔL), Step-Back and Net Displacement as a Function of Irradiation Position

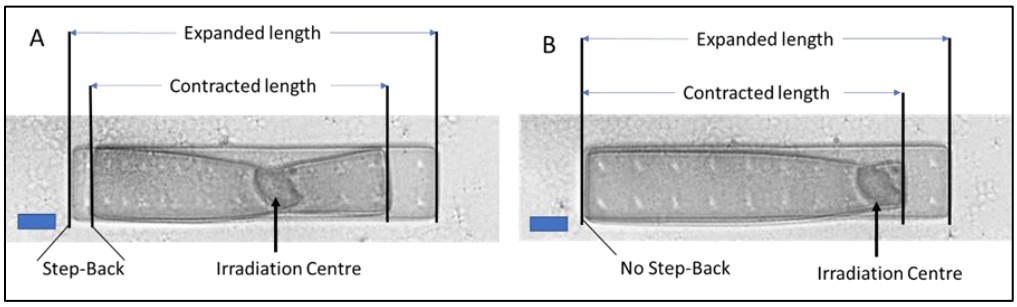

Figure 9) Images detailing the measurements of contraction, step-back and irradiation position. Scale bar = 25μm

By measuring the step-size (net displacement), contraction (ΔL) and step-back as a function of irradiation position, it is possible to build a clearer picture of how the mechanism leads to a net displacement and what limits the step-sizes. It can be seen on figure 8 that the step-sizes increase as the irradiation position moves on the particle from one end toward the midpoint. This can be explained by picturing the contracted area as having a maximum expansive force when the maximum amount of material is contracted. Qualitatively, this maximum occurs when the irradiation position is sufficiently far from the edges such that no material from the ends of the crawlers is contracted. Quantitatively, this is shown to be approximately 40 μm by figure 8. It can also be seen that as the irradiation position approaches the mid-point of the particle, the step-sizes decrease. Outside of the irradiation centre, material closer to the irradiation centre is pulled further towards the irradiation centre. This brings about a 'step-back' from the front side of the particle as the irradiation moves closer to the mid-point, hindering the net displacement. This is visible on figure 9A. This can be explained by visualising the direction of the forces of expansion. Any expansion that takes place pushes any non-actuating parts of the crawler away from the centre of expansion. This is due to the enhanced friction of the expanding section compared to the non-actuating, unchanged friction sections. If the contracted material is entirely on one half of the crawler, the expansion drives the other half away with the actuating side remaining relatively stationary, after the onset of the enhanced friction factor. That is to say, the more asymmetric the actuation, the greater the step-sizes. Thus, maximum step-sizes are found when the maximum amount of contracted material (ΔL) is balanced with sufficient asymmetry in the actuation (minimizing step-back). This is found to occur at approximately a third of the crawlers length from one end (figure 8).

Figure 8 also shows that the 100 µm crawlers demonstrate the greatest step sizes, followed by the 150 µm and then 220 µm crawlers. This provides evidence to support an earlier mentioned claim that increasing the total volume of the particle hinders the crawling mechanism. In the cases of all crawlers with the same width and sufficient length, the maximum amount of contracted material is the same. With the same expanding force, the resistive frictional force determines the net force and thus displacement of the crawler. It has been shown earlier that the friction force is proportional to the particles buoyant mass which is proportional the volume of the crawler. Thus, the step-sizes of the crawlers are limited by the total volume of the crawler. In the case of the crawlers of equal width; their length limits the step-sizes, which is shown in figure 8. It may be possible to overcome this limitation by simply upscaling the laser irradiation size and, thus, increase the amount of material contracting.

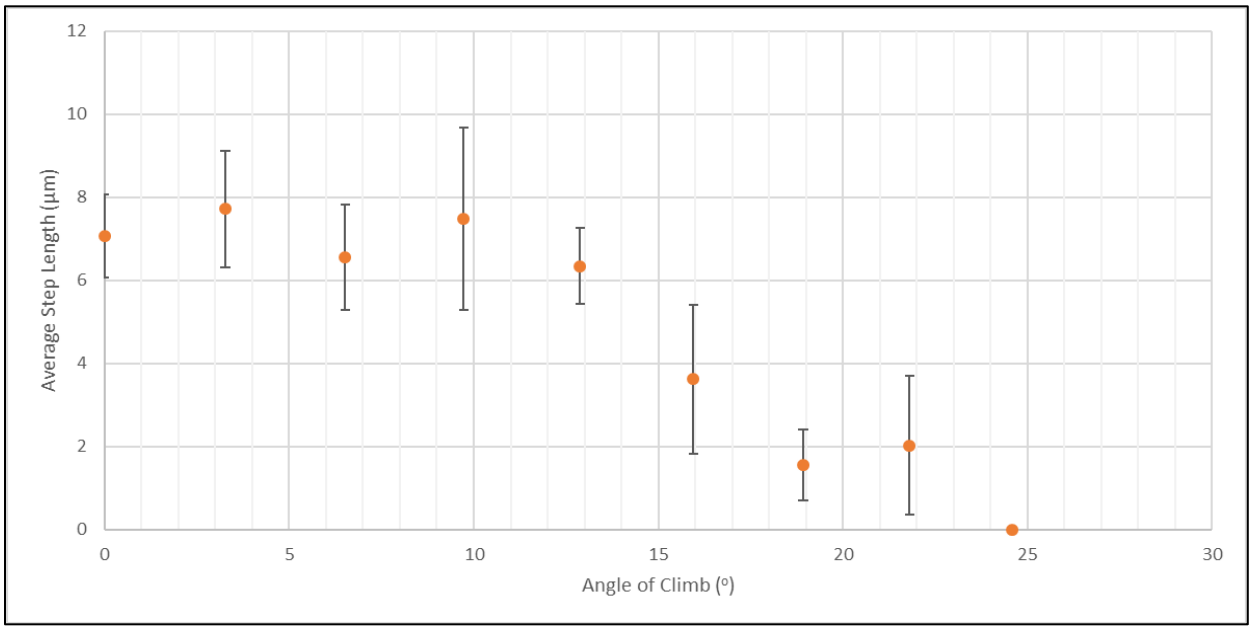

Figure 10) Plot of average step-sizes at increasing angles of climb.

By crawling uphill with the 100 µm x 50 µm crawlers, it is possible to estimate the force of expansion during each crawling step. Increasing the angle of the climb increases the lateral

gravitational force on the crawlers. Upon reaching an angle where the crawlers can no longer crawl uphill, the lateral force has exceeded the force exerted during each step. Thus, calculating the lateral force at the greatest angle for which the crawler can crawl gives an estimate for the force exerted during the steps. This is shown to be at 22° (figure 10) and thus the force exerted is estimated to be roughly ~15 pN (Appendix 2). The measurement is only an estimate as the experiment came with limitations. Firstly, at different angles, the irradiation of the particles is different as is shown figuratively in figure 11. Secondly, at the greater angles, some crawlers begin to slide downhill whilst others stay fixed to the surface. Crawling was thus only performed on the fixed crawlers which presents a significant bias in the measurements at greater angles. Nonetheless, it is remarkable that the angles the crawlers can climb up are greater than expected. It is a considerable step in robotic capability that the crawlers do not rely on a flat surface to crawl as it opens possibilities for the crawlers to navigate difficult environments.

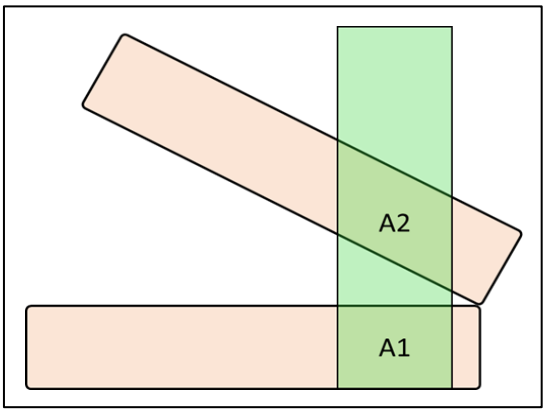

Figure 11) Demonstration of how illuminated volume differs upon increasing angle.

3.4 Steerable Crawling and Micromanipulation

Crawlers produced in the design depicted on 2.5.5.C can successfully crawl and be steered by the method proposed in section 2.5.4. By joining two parallel 150 µm x 50 µm crawlers (legs) with a 150 µm x 50 µm strip at their fronts, the crawler can be driven forward by alternating the actuation of the legs, or turn by actuating only one of the legs. By repeatedly actuating one leg, the crawlers turn 360° in a circular path. The crawlers were controlled to navigate between pieces of dirt on the surface over a direct path distance of approximately 1.5mm (10x the crawlers length) (figure 12).

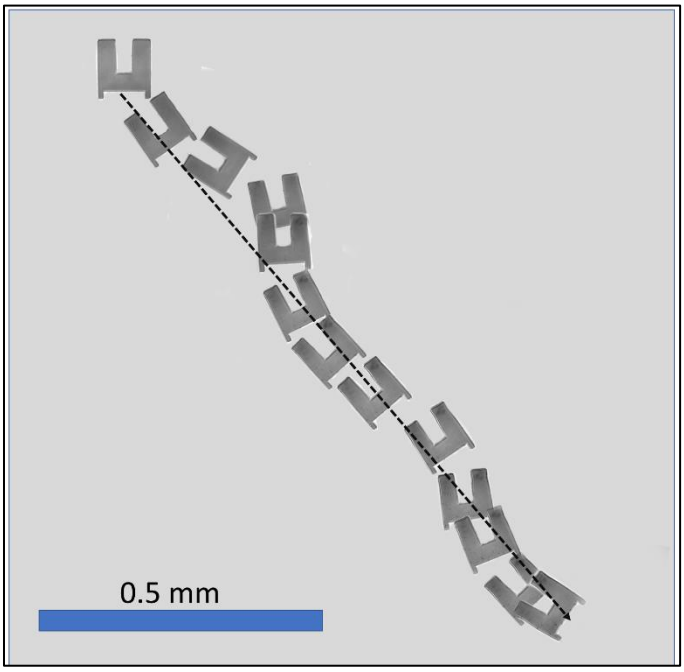

Figure 12) Combined images of steerable crawler navigating on a PDMS surface..

Using the steerable crawlers, 25 µm x 25 µm x 25 µm PEGDA cubes can be pushed easily and with precision i.e. it is possible to select one block, navigate to it and push it whilst avoiding other blocks present (figure 13). Large numbers of the blocks (up to 15) can be pushed by the crawlers, demonstrating their pushing force. However, attempts to form crystalline structures by

pushing large numbers of the cubes together with two crawlers were unsuccessful. The small antennae on either side of the front of the crawlers allow for the manipulation of large numbers of the cubes without them sliding off the front-side whilst turning. A mechanism for releasing the blocks was also discovered. By irradiating the middle of the front face, the front bends and the resulting stress imposed on the cubes by the antennae leads to them being released. Alternatively, the crawler can reverse away from the cubes by actuating the front corners, however, this is not very efficient and takes a much longer time than forward driving.

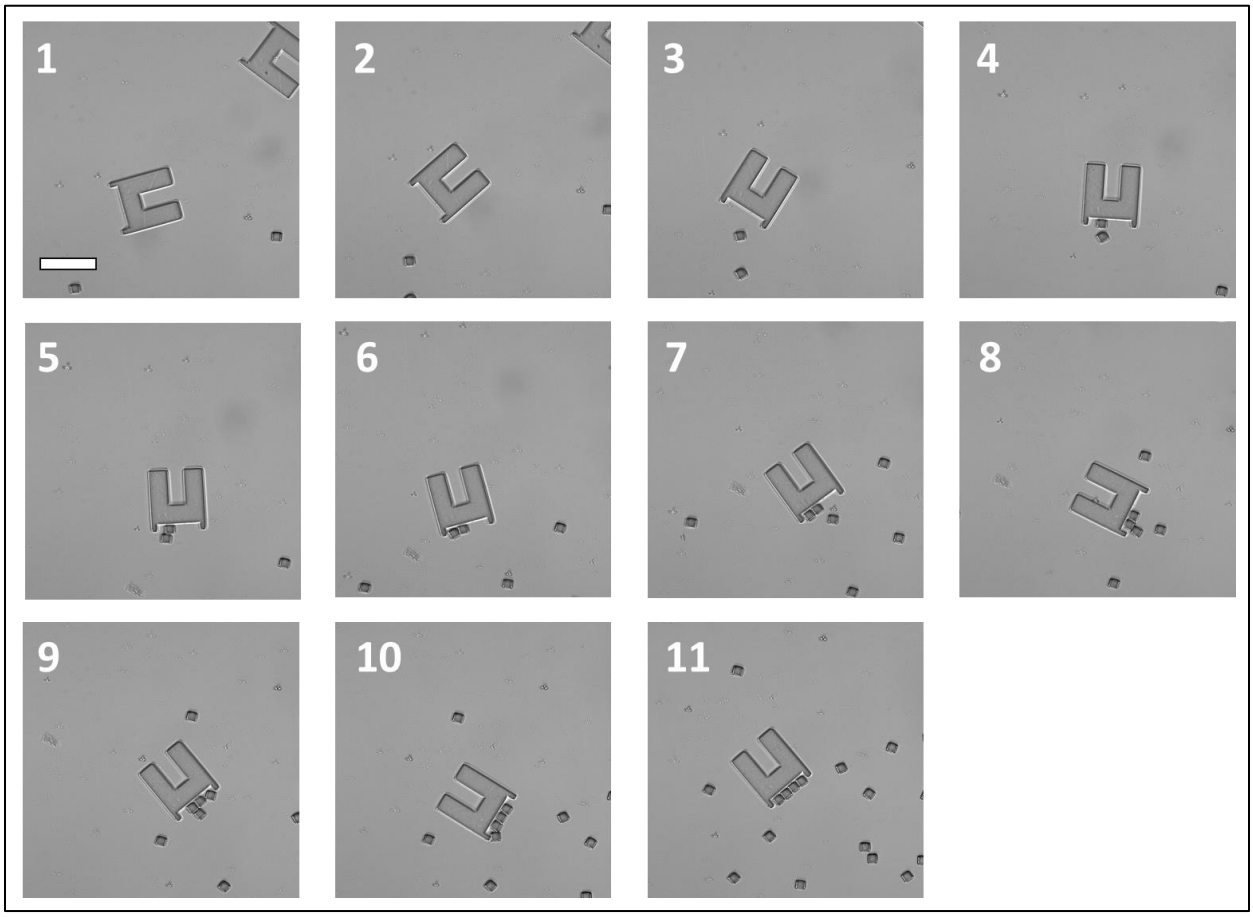

Figure 13) Sequence of steerable crawler selectively manipulating PEGDA blocks. Scale bar = 150 µm.

The crawlers ability to controllably manipulate the PEGDA blocks could have applications in many areas where micromanipulation is required. As previously discussed, their softness could

make them ideal for manipulating biological samples such as in single cell analysis or in-vitro fertilisation techniques[52]. Additionally, they may find applications in navigating microfluidic channels such as in lab-on-chip technologies. A hypothetical example is that they could be inserted into the channels to remove blockages or unwanted artefacts. One fortunate property of the crawlers is that they are most effective on PDMS which is commonly used in microfluidics[77].

3.5 Additional Results & Discussions

Notably, throughout this research there is inconsistency in the crawlers ability. It can be seen by the differing step-sizes at 0° for the uphill crawling experiments (figure 10) compared to the irradiation position experiments (figure 8) as well as the surface and surfactant measurements in the same conditions (Table 2 & 3; 0.5% w/w & PDMS respectively). This occurred regularly with different samples of the 100 μm x 50 μm crawlers in seemingly the same conditions, showing a range of step-sizes from no crawling to ~20 μm. This is thought to be a combination of a few synthetic factors. Firstly, the number density of the gold colloid in the pre-gel after preparation could vary depending on; the amount of supernatant removed after each centrifugation or by aggregations which would be non-photo-responsive or that would be sedimented in the final step. Secondly, pipetting such small quantities of viscous fluids such as PEGDA comes with imprecision which has an effect on the crosslinking density of the gels. It is unclear how the crosslinking density has an effect on the crawling ability by how it affects the elastic properties of the gel, though it is thought there is some correlation. Lastly, it may be possible that the PDMS surfaces deteriorated in some way after each use, possibly by; damage by the laser, a reaction to washing with ethanol and detergent, dust artefacts or residual surfactant. In future, samples should always be used with new spin-coated PDMS slides.

In order for the crawlers to be used as individual units in an active matter system, i.e. large numbers crawling simultaneously, two key design changes must be made. The first is to develop a way to globally heat the crawlers rather than photothermally heating them with a focussed laser and gold nanoparticles. The second is to produce the particles in SFL such that they are only responsive on one side, thus negating the need to aim the laser for asymmetric actuation. This can be realised easily by exploiting the laminar flow of two liquids in a microfluidic channel. If two inlets are used for the SFL, one containing photo-responsive pre-gel and the other non-functionalised PNIPAm (or an alternative polymer) pre-gel, then any photothermal heating will induce the asymmetric actuation without need for aiming. In their current form, only one crawler can be manipulated at one time with a powerfully focussed laser (50 mW / 100 μm^2 = 5 x 10^6 Wcm^{-2})[XII]. In order to have multiple crawlers moving at the same time, their sensitivity to the laser should be increased such that the laser need not be focussed to only one crawler. This was tested by using methylene-bis-acrylamide and lowering the PEGDA content of the pre-gel to decrease the crosslinking density (section 2.2.4). Of the mixtures tried, shown in table 1, mixtures 1 and 2 do not form homogenous gels in SFL and phase separate. It was thus decided to use mixture 3 as this was the lowest crosslinking that could form gels. The shrinking rate of two samples produced with different intensity UV light was measured. It is successful in lowering the crosslinking, as shown by a faster shrinking rate and smaller shrunken volume when heated externally (Appendix 4). However, due to the increased pore-sizes of lower cross-linked hydrogels, the gold nanoparticles quickly leak from the gels after they are formed and do not respond to laser

[XII] Calculated for the laser with the 0.5 OD filter.

illumination. To combat this, it was suggested to modify the gold particles with *bis*-acryloyl-cistamine to bind them to the network, though this was not empirically tested in this research.

Alternatively, new methods of photothermally heating the gels by embedding them with alternative nanoparticles for which higher intensity illumination methods are safe, such as infra-red. It was proposed to embed ferromagnetic nanoparticles into the gel, similarly to the gold nanoparticles, which would then be driven to vibrate thermally by an external oscillating magnetic field. This would be an excellent method for globally heating a sample of crawlers, however, calculations of the power required to heat the gels by more than 40°C indicate it is unfeasible with the equipment available.

Peristaltic actuation is also shown to induce motion with long crawlers (photomasks D, E and L). However, when considering the discovered friction modulation with PNIPAm it is hard to conclude whether the induced motion is indeed purely peristaltic. Additionally, methods of actuating the crawlers that rely on pulses of lasers longer than 1 second, as is needed for peristaltic motion, induce convection in the liquid by the heat of the laser beam. The convection leads to the particles drifting on the surface, dramatically effecting displacement measurements. As such, no conclusive statements could be made regarding the peristaltic motion.

The attempts to achieve crawling by ratcheting the particles (2.5.1.1) were unsuccessful due to the limits of the SFL procedure. The particles produced from photomask M fall on to their smooth sides and so there is no inherent directionality to their friction. The ratcheted particles produced with photomask L lie with the ratchet side on the surface and are shown to crawl by off-centre actuation. However, the effect of the ratcheting was considered negligible as the particles are shown to crawl with and against the direction given by the ratchet. It is thus concluded that if crawling is demonstrated with ratcheted particles, it is via the principle mechanism.

4 Conclusions and Outlook

In this research, a new locomotion principle for soft robots has been discovered and applied on a micro-scale. By exploiting the friction hysteresis of PNIPAm hydrogels during shrinking and expanding cycles, the gels can crawl by coupling this phenomenon to reciprocal actuation. The hysteresis is inherent to the PNIPAm and so crawlers can be produced in many designs, giving them extra abilities such as steerability. The continuous method of production, stop-flow lithography, is cheap, simple to realise and could easily be scaled up by orders of magnitude to produce industrial quantities of the crawlers. Furthermore, improvements and/or modifications to the design may allow the production of simultaneously responsive and functional crawlers. Such large groups of micro-crawlers, functionalised to grab or deposit cargos, could be powerful tools in medicine, defence and micro-construction. The actuation by focussed laser light is the current limiting factor and so research should now be directed towards modifying the crawlers to be responsive to safer or less intense stimuli.

Acknowledgements

The author would like to offer their immense gratitude to Ivan Rehor, Burak Eral and Willem Kegel for enabling such a fascinating research project. To Ivan, particularly, for his limitless supply of knowledge and experimental expertise that was shared during the project and which was the key driver of the research. To Willem and Burak, for their calming influence and encouragement. Additional thanks must go to Pepijn Moerman, Jan Groenewald and Jasper Landman whose contributions in discussion were key to the progress of the project. Finally, to all staff and students of the Van ’t Hoff Laboratory, the author sends their warmest regards and thanks for such an enjoyable time.

References

1. Ilievski, F., Mazzeo, A. D., Shepherd, R. F., Chen, X. & Whitesides, G. M. Soft Robotics for Chemists. *Angew. Chem. Int. Ed.* **50,** 1890–1895 (2011).
2. Vaddiraju, S., Tomazos, I., Burgess, D. J., Jain, F. C. & Papadimitrakopoulos, F. Emerging synergy between nanotechnology and implantable biosensors: A review. *Biosens. Bioelectron.* **25,** 1553–1565 (2010).
3. Hsu, T.-R. *MEMS and Microsystems: Design, Manufacture, and Nanoscale Engineering*. (John Wiley & Sons, 2008).
4. Shen, Q., Arae, D. & Toyoda, T. Photosensitization of nanostructured TiO2 with CdSe quantum dots: effects of microstructure and electron transport in TiO2 substrates. *J. Photochem. Photobiol. Chem.* **164,** 75–80 (2004).
5. Marchetti, M. C. *et al.* Soft Active Matter. *ArXiv12072929 Cond-Mat Q-Bio* (2012).
6. Bechinger, C. *et al.* Active particles in complex and crowded environments. *Rev. Mod. Phys.* **88,** 045006 (2016).
7. Goldstein, J. Emergence as a Construct: History and Issues. *Emergence* **1,** 49–72 (1999).
8. Yu, C. *et al.* Electronically Programmable, Reversible Shape Change in Two- and Three-Dimensional Hydrogel Structures. *Adv. Mater.* **25,** 1541–1546 (2013).
9. Majidi, C. Soft Robotics: A Perspective—Current Trends and Prospects for the Future. *Soft Robot.* **1,** 5–11 (2013).
10. Savage, N. Soft robots for hard problems. *IEEE Spectr.* **49,** 13–13 (2012).
11. Anderson, R. C., Mather, J. A. & Wood, J. B. *Octopus: The Ocean's Intelligent Invertebrate*. (Timber Press, 2013).

12. Noselli, G., Tatone, A. & DeSimone, A. Discrete one-dimensional crawlers on viscous substrates: Achievable net displacements and their energy cost. *Mech. Res. Commun.* **58,** 73–81 (2014).
13. Behn, C., Zeidis, I. & Zimmermann, K. *Mechanics of Terrestrial Locomotion*. (Springer Berlin Heidelberg). doi:10.1007/978-3-540-88841-3
14. Plaut, R. H. Mathematical model of inchworm locomotion. *Int. J. Non-Linear Mech.* **76,** 56–63 (2015).
15. Ueno, S., Takemura, K., Yokota, S. & Edamura, K. Micro inchworm robot using electro-conjugate fluid. *Sens. Actuators Phys.* **216,** 36–42 (2014).
16. Dubey, S., Prateek, M. & Saxena, M. Robot Locomotion-A Review. *Int. J. Appl. Eng. Res.* **10,** 7357–69 (2015).
17. Osada, Y., Okuzaki, H. & Hori, H. A polymer gel with electrically driven motility. *Nature* **355,** 242–244 (1992).
18. Morales, D., Palleau, E., Dickey, M. D. & Velev, O. D. Electro-actuated hydrogel walkers with dual responsive legs. *Soft Matter* **10,** 1337–1348 (2014).
19. Maeda, S., Hara, Y., Sakai, T., Yoshida, R. & Hashimoto, S. Self-Walking Gel. *Adv. Mater.* **19,** 3480–3484 (2007).
20. Yang, C. *et al.* Hydrogel Walkers with Electro-Driven Motility for Cargo Transport. *Sci. Rep.* **5,** 13622 (2015).
21. Hill, C., Amodeo, A., Joseph, J. V. & Patel, H. R. Nano- and microrobotics: how far is the reality? *Expert Rev. Anticancer Ther.* **8,** 1891–1897 (2008).
22. Ullrich, F. *et al.* Recent Progress in Magnetically Actuated Microrobotics for Ophthalmic Therapies. *Eur. Ophthalmic Rev.* **08,** 120 (2014).

23. Menciassi, A., Quirini, M. & Dario, P. Microrobotics for future gastrointestinal endoscopy. *Minim. Invasive Ther. Allied Technol.* **16,** 91–100 (2007).
24. Zhang, H., Hutmacher, D. W., Chollet, F., Poo, A. N. & Burdet, E. Microrobotics and MEMS-Based Fabrication Techniques for Scaffold-Based Tissue Engineering. *Macromol. Biosci.* **5,** 477–489 (2005).
25. Guven, S. *et al.* Multiscale assembly for tissue engineering and regenerative medicine. *Trends Biotechnol.* **33,** 269–279 (2015).
26. Lu, T., Li, Y. & Chen, T. Techniques for fabrication and construction of three-dimensional scaffolds for tissue engineering. *Int. J. Nanomedicine* **8,** 337–350 (2013).
27. *Natural Locomotion in Fluids and on Surfaces*. **155,** (Springer New York, 2012).
28. Purcell, E. M. Life at low Reynolds number. *Am. J. Phys.* **45,** 3–11 (1977).
29. Pelton, R. Poly(N-isopropylacrylamide) (PNIPAM) is never hydrophobic. *J. Colloid Interface Sci.* **348,** 673–674 (2010).
30. Yamauchi, H. & Maeda, Y. LCST and UCST Behavior of Poly(N-isopropylacrylamide) in DMSO/Water Mixed Solvents Studied by IR and Micro-Raman Spectroscopy. *J. Phys. Chem. B* **111,** 12964–12968 (2007).
31. Maeda, Y., Higuchi, T. & Ikeda, I. Change in Hydration State during the Coil−Globule Transition of Aqueous Solutions of Poly(N-isopropylacrylamide) as Evidenced by FTIR Spectroscopy. *Langmuir* **16,** 7503–7509 (2000).
32. Graziano, G. On the temperature-induced coil to globule transition of poly-N-isopropylacrylamide in dilute aqueous solutions. *Int. J. Biol. Macromol.* **27,** 89–97 (2000).

33. NIPAM based Polymers. *Sigma-Aldrich* Available at: https://www.sigmaaldrich.com/materials-science/polymer-science/nipam-polymers.html. (Accessed: 17th January 2018)
34. Son, K. H. & Lee, J. W. Synthesis and Characterization of Poly(Ethylene Glycol) Based Thermo-Responsive Hydrogels for Cell Sheet Engineering. *Materials* **9,** 854 (2016).
35. Yi, G. *et al.* Preparation and swelling behaviors of rapid responsive semi-IPN NaCMC/PNIPAm hydrogels. *J. Wuhan Univ. Technol.-Mater Sci Ed* **26,** 1073–1078 (2011).
36. Depa, K., Strachota, A., Šlouf, M. & Hromádková, J. Fast temperature-responsive nanocomposite PNIPAM hydrogels with controlled pore wall thickness: Force and rate of T-response. *Eur. Polym. J.* **48,** 1997–2007 (2012).
37. Sershen, S. R. *et al.* Independent Optical Control of Microfluidic Valves Formed from Optomechanically Responsive Nanocomposite Hydrogels. *Adv. Mater.* **17,** 1366–1368 (2005).
38. Cai, S. & Suo, Z. Mechanics and chemical thermodynamics of phase transition in temperature-sensitive hydrogels. *J. Mech. Phys. Solids* **59,** 2259–2278 (2011).
39. Tian, H., Tang, Z., Zhuang, X., Chen, X. & Jing, X. Biodegradable synthetic polymers: Preparation, functionalization and biomedical application. *Prog. Polym. Sci.* **37,** 237–280 (2012).
40. Kreibig, U. & Vollmer, M. *Optical Properties of Metal Clusters*. (Springer Science & Business Media, 2013).
41. Grzelczak, M. & Liz-Marzán, L. M. Colloidal Nanoplasmonics: From Building Blocks to Sensing Devices. *Langmuir* **29,** 4652–4663 (2013).

42. Sershen, S. R., Westcott, S. L., Halas, N. J. & West, J. L. Temperature-sensitive polymer–nanoshell composites for photothermally modulated drug delivery. *J. Biomed. Mater. Res.* **51,** 293–298 (2000).

43. Su, K.-H. *et al.* Interparticle Coupling Effects on Plasmon Resonances of Nanogold Particles. *Nano Lett.* **3,** 1087–1090 (2003).

44. Shubitidze, F., Kekalo, K., Stigliano, R. & Baker, I. Magnetic nanoparticles with high specific absorption rate of electromagnetic energy at low field strength for hyperthermia therapy. *J. Appl. Phys.* **117,** (2015).

45. Breger, J. C. *et al.* Self-Folding Thermo-Magnetically Responsive Soft Microgrippers. *ACS Appl. Mater. Interfaces* **7,** 3398–3405 (2015).

46. Backes, S. *et al.* Loading of PNIPAM Based Microgels with $CoFe_2O_4$ Nanoparticles and Their Magnetic Response in Bulk and at Surfaces. *J. Phys. Chem. B* **119,** 12129–12137 (2015).

47. actuation Meaning in the Cambridge English Dictionary. Available at: https://dictionary.cambridge.org/dictionary/english/actuation. (Accessed: 21st January 2018)

48. Kim, J., Hanna, J. A., Byun, M., Santangelo, C. D. & Hayward, R. C. Designing responsive buckled surfaces by halftone gel lithography. *Science* **335,** 1201–1205 (2012).

49. Guo, W., Li, M. & Zhou, J. Modeling programmable deformation of self-folding all-polymer structures with temperature-sensitive hydrogels. *Smart Mater. Struct.* **22,** 115028 (2013).

50. Stoychev, G., Puretskiy, N. & Ionov, L. Self-folding all-polymer thermoresponsive microcapsules. *Soft Matter* **7,** 3277–3279 (2011).

51. Yoon, C. *et al.* Functional stimuli responsive hydrogel devices by self-folding. *Smart Mater. Struct.* **23,** 094008 (2014).

52. Pelah, A., Seemann, R. & Jovin, T. M. Reversible Cell Deformation by a Polymeric Actuator. *J. Am. Chem. Soc.* **129,** 468–469 (2007).

53. Hoare, T. R. & Kohane, D. S. Hydrogels in drug delivery: Progress and challenges. *Polymer* **49,** 1993–2007 (2008).

54. Chastek, T., Wadajkar, A., Nguyen, K. T., Hudson, S. D. & Chastek, T. Q. Improving the Biocompatibility of Thermo-Sensitive Poly(N-Isopropyl Acrylamide) Nanoparticles for Drug Delivery. *Biomaterials* **288,** (2009).

55. Shiotani, A., Mori, T., Niidome, T., Niidome, Y. & Katayama, Y. Stable Incorporation of Gold Nanorods into N-Isopropylacrylamide Hydrogels and Their Rapid Shrinkage Induced by Near-Infrared Laser Irradiation. *Langmuir* **23,** 4012–4018 (2007).

56. Yamashita, K., Nishimura, T. & Nango, M. Preparation of IPN-type stimuli-Responsive heavy-Metal-Ion adsorbent gel. *Polym. Adv. Technol.* **14,** 189–194 (2003).

57. Cheng, J., Shan, G. & Pan, P. Temperature and pH-dependent swelling and copper(II) adsorption of poly(N-isopropylacrylamide) copolymer hydrogel. *RSC Adv.* **5,** 62091–62100 (2015).

58. Dendukuri, D., S. Gu, S., C. Pregibon, D., Alan Hatton, T. & S. Doyle, P. Stop-flow lithography in a microfluidic device. *Lab. Chip* **7,** 818–828 (2007).

59. Pregibon, D. C., Toner, M. & Doyle, P. S. Multifunctional encoded particles for high-throughput biomolecule analysis. *Science* **315,** 1393–1396 (2007).

60. Bong, K. W., Bong, K. T., Pregibon, D. C. & Doyle, P. S. Hydrodynamic Focusing Lithography. *Angew. Chem. Int. Ed.* **49,** 87–90 (2010).

61. Appleyard, D. C., Chapin, S. C., Srinivas, R. L. & Doyle, P. S. Bar-coded hydrogel microparticles for protein detection: synthesis, assay and scanning. *Nat. Protoc.* **6,** 1761–1774 (2011).
62. Suh, S. K. *et al.* Synthesis of Nonspherical Superparamagnetic Particles: In Situ Coprecipitation of Magnetic Nanoparticles in Microgels Prepared by Stop-Flow Lithography. *J. Am. Chem. Soc.* **134,** 7337–7343 (2012).
63. Rivest et al. Microscale hydrogels for medicine and biology: synthesis, characteristics and applications. *J. Mech. Mater. Struct.* **2,** 1103–1119 (2007).
64. Yeh, J. *et al.* Micromolding of shape-controlled, harvestable cell-laden hydrogels. *Biomaterials* **27,** 5391–5398 (2006).
65. Ma, C., Tian, C., Zhao, L. & Wang, J. Pneumatic-aided micro-molding for flexible fabrication of homogeneous and heterogeneous cell-laden microgels. *Lab. Chip* **16,** 2609–2617 (2016).
66. Dendukuri, D., Pregibon, D. C., Collins, J., Hatton, T. A. & Doyle, P. S. Continuous-flow lithography for high-throughput microparticle synthesis. *Nat. Mater.* **5,** 365 (2006).
67. Lee, K.-S., Kim, R. H., Yang, D.-Y. & Park, S. H. Advances in 3D nano/microfabrication using two-photon initiated polymerization. *Prog. Polym. Sci.* **33,** 631–681 (2008).
68. Niesler, F. & Hermatschweiler, M. Two-Photon Polymerization — A Versatile Microfabrication Tool. *Laser Tech. J.* **12,** 44–47 (2015).
69. Cumpston, B. H. *et al.* Three-dimensional microfabrication using two-photon polymerization. in **3512,** 168–168 (1998).
70. Frens, G. Controlled Nucleation for the Regulation of the Particle Size in Monodisperse Gold Suspensions. *Nat. Phys. Sci.* **241,** 20 (1973).

71. Vetter, R., Stoop, N., Wittel, F. K. & Herrmann, H. J. Simulating Thin Sheets: Buckling, Wrinkling, Folding and Growth. *J. Phys. Conf. Ser.* **487,** 012012 (2014).
72. Yu, Y. *et al.* Tunable friction by employment of co-non-solvency of PNIPAM brushes. *Polymer* **102,** 372–378 (2016).
73. Yu, Y. *et al.* Stretching of collapsed polymers causes an enhanced dissipative response of PNIPAM brushes near their LCST. *Soft Matter* **11,** 8508–8516 (2015).
74. Liu, G. & Zhang, G. Collapse and Swelling of Thermally Sensitive Poly(N-isopropylacrylamide) Brushes Monitored with a Quartz Crystal Microbalance. *J. Phys. Chem. B* **109,** 743–747 (2005).
75. Cheng, H., Liu, G., Wang, C., Zhang, G. & Wu, C. Collapse and swelling of poly(N-isopropylacrylamide-co-sodium acrylate) copolymer brushes grafted on a flat SiO2 surface. *J. Polym. Sci. Part B Polym. Phys.* **44,** 770–778 (2006).
76. LeMoyne, R. *Advances for Prosthetic Technology: From Historical Perspective to Current Status to Future Application*. (Springer, 2016).
77. Berg, A. van den, G. Craighead, H. & Yang, P. From microfluidic applications to nanofluidic phenomena. *Chem. Soc. Rev.* **39,** 899–900 (2010).

Appendix

1. Calculation of Number Density of the Gold Colloid.

300 µL of the $HAuCl_4$ solution weighs 0.3 g, of which 0.003 (1% mass w/w) is $HAuCl_4$.

The M_w of $HAuCl_4$ is 339.8 $gmol^{-1}$.

Thus, there is (0.003 g/ 339.8 $gmol^{-1}$ =) 8.83 x 10^{-6} mol of gold in the solution.

The atomic weight of gold is 197 $gmol^{-1}$.

Thus, there is (8.83x10^{-6} g x 197 $gmol^{-1-}$ =) 0.001739 g of gold in the solution.

The volume of a 15 nm diameter sphere is ((4/3) x π x (7.5x10^{-9})^3 =) 1.77x10^{-24} m^3.

The density of gold is 19.3x10^6 gm^{-3}.

Thus, one sphere of gold weighs (19. 3x10^6 gm^{-3} x 1.77x10^{-24} m^3 =) 3.41 x 10^{-17} g.

The number of gold spheres in the 30 cm^3 solution is then the total mass of gold in solution (0.001739 g) divided by the mass of one sphere (3.41 x 10^{-17} g) = 5.10x10^{13}. The number density per m^3 is then (5.10x10^{13} / 30x10^{-6} =) 1.70x10^{18} m^{-3}.

After centrifuging down to 100 µL and assuming zero losses of the colloid, the number density is then (5.10x10^{13} / 100x10^{-9} =) 5.10x10^{20} m^{-3}.

Assuming the spheres are homogenously distributed at this number density in the gel, then each occupies a cubic volume of (1 / 5.10x10^{20} =) 1.96x10^{-21} m^3.

The cube root of this volume minus the particles diameter is then the interparticle distance.

$\sqrt[3]{}$(1.96x10^{-21} m^3) – 15x10^{-9} m = 1.10x10^{-7} m = 1100 nm.

If the gel contracts to 50% of it's volume, the interparticle distance will decrease to 550 nm.

This distance is large enough to not cause any interparticle plasmonic interference effects [43].

2. Calculation of Normal Load on Particles in Uphill and Crawling Experiments.

   Density of water: $\rho_{water} = 1 \times 10^3$ kgm^{-3}

   Density of dry PNIPAm: $\rho_{PNIPAm} = 1.1 \times 10^3$ kgm^{-3}

   As the gel is 2/3 water, the buoyant density is then: $1/3 \times 0.1 \times 10^3$ kgm^{-3} = 30 kgm^{-3}.

   Volume of a 100 x 50 crawler: $V_{crawler} = (100 \times 50 \times 25) \times (10^{-6})^3$ m^3 = 1.25×10^{-13} m^3.

   Mass of the crawler: $m_{crawler} = V_{crawler} \times 30$ kgm^{-3} = 3.75×10^{-12} kg.

   Force due to gravity is then: $m_{crawler} \times g = 3.67 \times 10^{-11}$ = 36.7 pN.

   At an angle of 22°, lateral force on the crawler is: 36.7 pN x sin(22°) = 13.8 pN.

3. Shrinking Responses of Gels Produced with Mix 3.

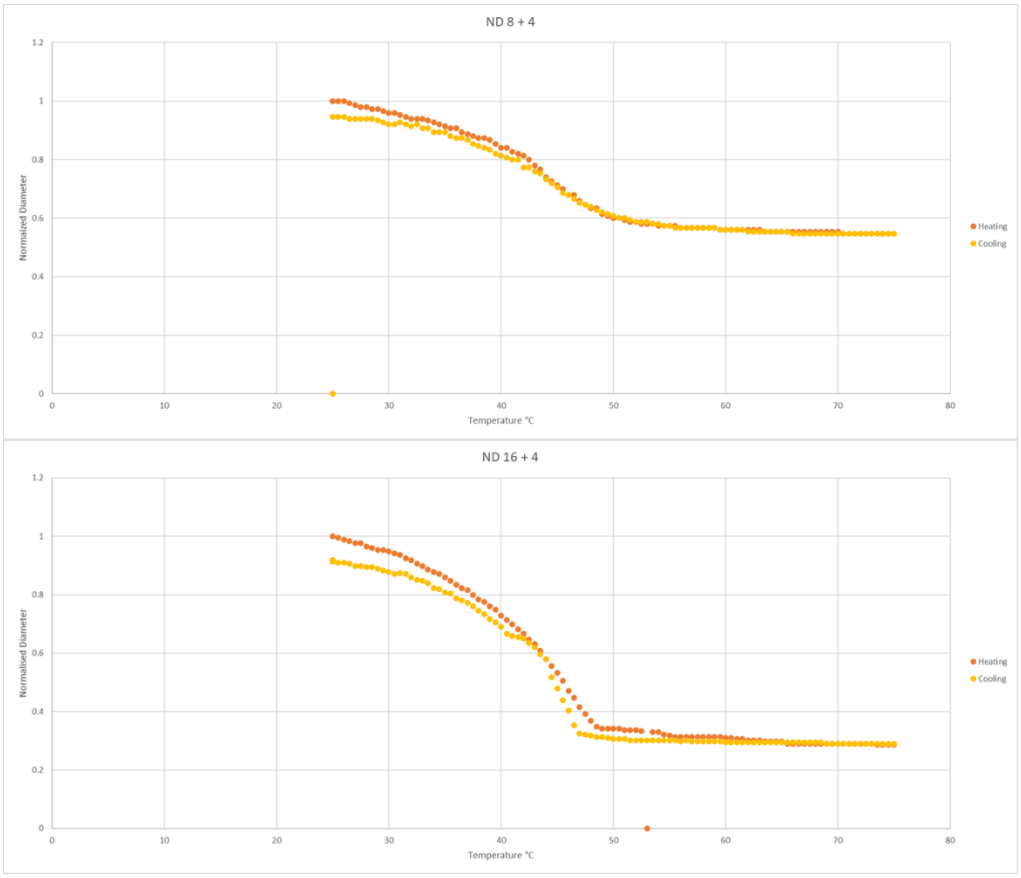

4. Experimental Set-ups

(i) 200 mW 532 nm laser fitted with 4 LEDs.

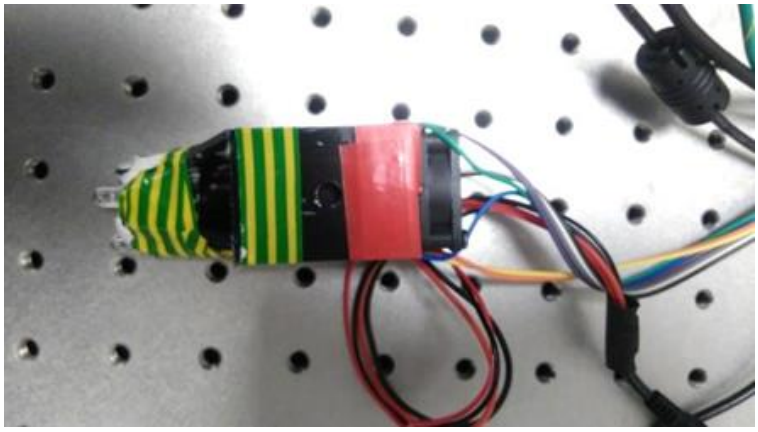

(ii) Microscope set-up with laser focussed by the Condenser lens.

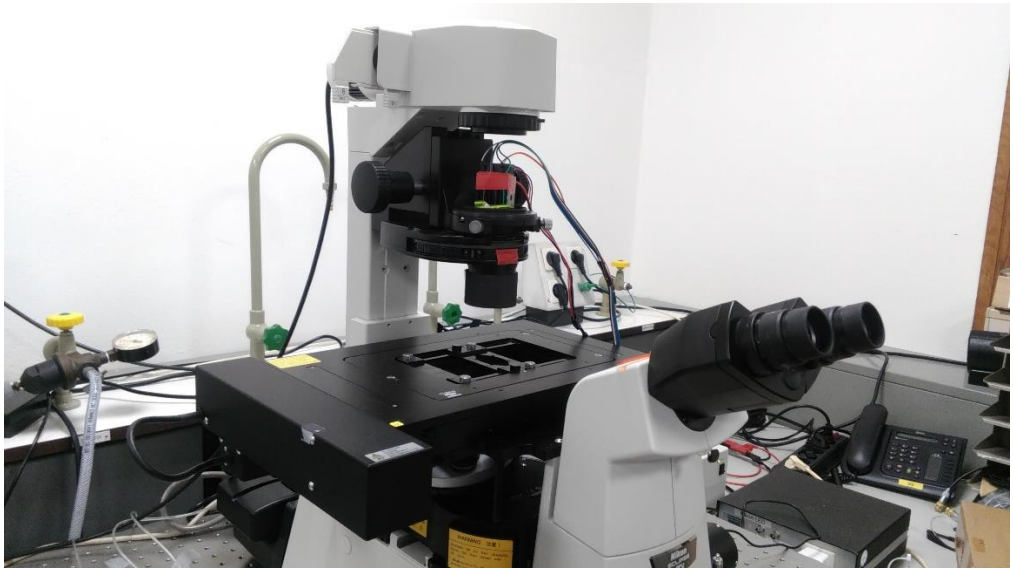

(iii) PDMS wells for observation and control.

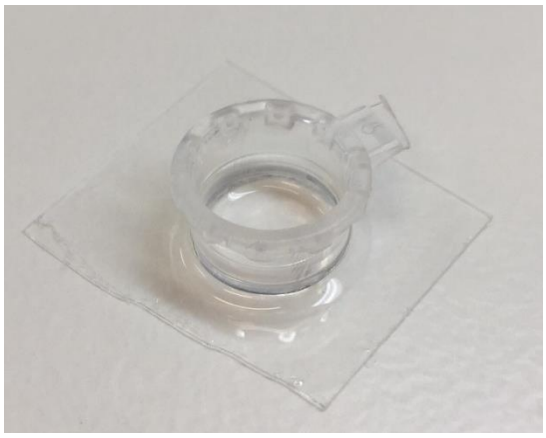

(iv) Experimental set-up for experiment 2.5.2.2: tilted microscope and heating stage.

(v) Microfluidic chip with inlet and outlet ports.